Some rotational corrections to the acoustic energy equation in injection-driven enclosures

J. Majdalani,[a] G. A. Flandro, and S. R. Fischbach
Department of Mechanical, Aerospace and Biomedical Engineering, University of Tennessee Space Institute (UTSI), 411 B.H. Goethert Parkway, MS-23, Tullahoma, Tennessee 37388-9700

(Received 20 December 2004; accepted 14 March 2005; published online 27 June 2005)

This article presents rotational corrections to the energy stability equation in injection-driven porous enclosures used to simulate solid rocket motors. The evaluation of stability growth rate factors is carried out both numerically and asymptotically. Analytical expressions for the energy stability factors are obtained over a spectrum of physical parameters encompassing solid rocket motor operation. For all representative motors under investigation, the analytical estimates are shown to exhibit negligible errors compared to their numerical values. Both numerics and asymptotics converge in predicting less stable systems than projected by purely irrotational stability theory. The differences can be ascribed to the dismissal of time-dependent rotational coupling in some past formulations. The current study unravels the details of six additional growth rate corrections not accounted for previously. These include the rotational flow, inviscid vortical, viscous, pseudoacoustical, pseudorotational, and unsteady nozzle growth rate factors. The fourth and fifth terms are due to acoustical and vortical interactions with the often neglected pseudopressure. The sixth is due to the energy associated with the unsteady rotational flow exiting the porous enclosure. This study enables us to explain the influence of distinct flow variables on stability. Based on asymptotic approximations for individual growth rates, explicit criteria are presented in the form of critical Mach numbers, penetration numbers, or motor lengths that must not be exceeded in prevention of system instability. The net rotational corrections have been recently appended to the widely used Standard Stability Prediction code. © *2005 American Institute of Physics*.
[DOI: 10.1063/1.1920647]

I. INTRODUCTION

For reasons not entirely understood, combustion chambers that favor high efficiencies and low emissions are prone to combustion instabilities. These instabilities arise due to a regenerative coupling between chamber acoustics and propellant burning. Instabilities generally appear as self-excited limit cycle oscillations in the flow variables inside both propulsion and power generation systems. These include ramjet engines, rocket motors, gas turbines, preburners, afterburners, and large industrial combustors. A plethora of names has appeared to describe these oscillations—humming, screeching, buzzing, and rumbling, to name a few.

In principle, these oscillations can be separated into three distinct wave types also known as "fluctuation modes." The three modes include acoustical (pressure-driven), vortical (boundary-driven), and thermal (entropy-driven) disturbances.[1] The term "combustion" instability has been routinely used to denote instabilities in the acoustical waves. Corresponding oscillations have often been shown to produce pressure amplitudes large enough to cause severe structural damage or outright system failure.

In light of these concerns, considerable attention has been given to the prediction of acoustic instabilities in solid rocket motors. One of the major contributors to the field is Culick[2–6] whose papers on flow instability published in the early 1970s are rightfully perceived as the foundation for all stability prediction schemes.[7,8] Culick's approach considers small amplitude pressure fluctuations, thin combustion zone, and one-dimensional acoustic waves to model the unsteady core flow.[3] Based on this paradigm, several predictive codes have been developed, including the widely used Standard Stability Prediction (SSP) program.[9–11]

Realizing the inability of one-dimensional waves to allow for three-dimensional interactions with solid boundaries, Culick later proposed rotational corrections that could be applied retroactively to improve the accuracy of existing stability formulations.[12] The flow turning loss is one such correction that has later become the subject of debate. As noted by Flandro,[13] there have been numerous cases for which the flow turning loss has led to less favorable predictions. Rotational corrections were thus suggested that could be readily incorporated into Culick's algorithm.

The last decade has given rise to significant improvements in the general understanding of rotationality and core flow dynamics.[14] Analytical,[13–22] numerical,[23–28] and experimental studies[29–32] have jointly confirmed the essential contributions of pressure- and boundary-driven vortico-acoustic waves. These new findings have triggered a growing trend in the acoustic instability community to incorporate vortical effects in order to refine the irrotational representation of the system energy balance.

By way of example, the controversy surrounding the

[a]Author to whom correspondence should be addressed. Fax: (931) 393-7333. Electronic mail: maji@utsi.edu

flow turning loss was discussed in a former study by Flandro and Majdalani.[33] The key was to include the unsteady rotational terms at the start, and then retain them consistently throughout the energy assessment. By so doing, several additional correction factors could be unraveled, and most of those were presented to leading order in this earlier work.[33] Among the newly determined corrections were factors that either canceled the flow turning loss or suggested new destabilizing agents. The cancellation of the flow turning loss explained its adverse role when employed as a retroactive fix in certain rocket motor simulations. It also confirmed the mathematical proof furnished by Van Moorhem[34,35] who circumscribed the flow turning loss to one-dimensional models; this followed a formal analysis showing that flow turning would strictly vanish in two- and three-dimensional representations. The emergence of new terms, on the other hand, justified the presence of additional sources and sinks of unsteady energy that could not be captured without rotational terms being allowed into the energy balance equation.

The current article extends the former study by Flandro and Majdalani[33] whose focus has been on identifying new growth rate expressions resulting from the inclusion of rotational waves. Considering that the former article was chiefly concerned with producing fundamental expressions for the stability growth rate factors, the role of this article is to provide the mathematical steps needed to arrive at higher-order growth rate expressions for the purpose of approximating the numerically simulated integrals. In the process, special attention will be given to the pseudopressure corrections which have been found to be important in recent experimental and numerical rocket motor simulations.[36–40] Furthermore, the unsteady energy crossing the exit plane will be accounted for. This will lead to a loss term that causes the cancellation of the pseudorotational growth rate. After producing explicit approximations for the linear growth rates, criteria delineating motor stability will be furnished in closed form.

Insofar as these calculations rely on volume integrals of time-dependent pressure and velocity distributions, the one-term approximation based on Flandro's original solution will be used to define the unsteady flow component.[13] Although higher-order expressions for the mean flow are available (cf. Majdalani, Flandro, and Roh[17]), the unsteady flow approximation used here will permit simple solutions for the growth rate factors. In light of this, the impact of varying a motor's aspect ratio, oscillation mode number, viscosity, surface admittance, and Mach number will be illuminated. The quest for a higher-order approximation will also permit the assessment of instability emergence and growth over a broad spectrum of physical settings.

II. BASIC MODEL AND FORMULATION

Culick's mean flow model[3] for an internal burning tube is adopted in the current analysis with the coordinate system shown in Fig. 1. Flandro's leading-order solution for the unsteady flow is also used to represent the unsteady rotational and acoustic disturbances.[13,14,17] The mean velocity comprises both radial and axial components, namely,

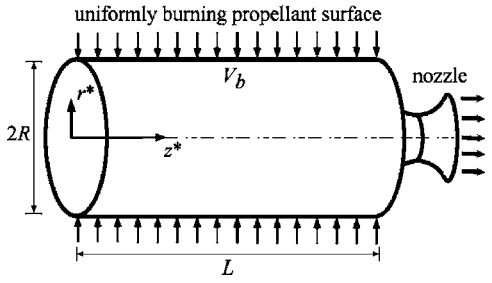

FIG. 1. Idealized motor chamber and its coordinate system.

$$\mathbf{U} = U_r\mathbf{e}_r + U_z\mathbf{e}_z = -r^{-1}\sin(x)\mathbf{e}_r + \pi z\cos(x)\mathbf{e}_z, \tag{1}$$

where $x \equiv \frac{1}{2}\pi r^2$ recurs frequently. The linearized continuity and momentum equations become

$$\frac{\partial \rho^{(1)}}{\partial t} + \nabla\cdot\mathbf{u}^{(1)} = -M_b\mathbf{U}\cdot\nabla\rho^{(1)}, \tag{2}$$

$$\frac{\partial \mathbf{u}^{(1)}}{\partial t} + \nabla p^{(1)} = M_b\{\mathbf{u}^{(1)}\times(\nabla\times\mathbf{U}) + \mathbf{U}\times[\nabla\times\mathbf{u}^{(1)}] - \nabla[\mathbf{U}\cdot\mathbf{u}^{(1)}]\} + \delta^2\left\{\tfrac{4}{3}\nabla[\nabla\cdot\mathbf{u}^{(1)}] - \nabla\times[\nabla\times\mathbf{u}^{(1)}]\right\}, \tag{3}$$

where ρ is the density, $\mathbf{u}$ is the total velocity vector, and the second coefficient of viscosity is taken to be $-\frac{2}{3}\mu$. Note that the energy equation is not considered here due to the small influence of thermal disturbances on acoustic instability and the small thickness of the flame zone.[41,42] The superscript (1) denotes first-order terms in the perturbation parameter, $\varepsilon = A_p/(\gamma p_0)$; here A_p is the unsteady pressure amplitude, p_0 is the mean pressure, and γ is the ratio of specific heats. A second small parameter, the mean flow Mach number at the burning surface, is given by $M_b = V_b/a_0$; as usual V_b is the burning velocity and a_0 is the mean speed of sound; this parameter is also used in the linearization process. All variables are represented as combinations of irrotational and rotational contributions, viz.,

$$p^{(1)} = \hat{p}^{(1)} + \tilde{p}^{(1)}, \quad \rho^{(1)} = \hat{\rho}^{(1)}, \quad \mathbf{u}^{(1)} = \hat{\mathbf{u}}^{(1)} + \tilde{\mathbf{u}}^{(1)}. \tag{4}$$

In general, the caret (^) will denote the irrotational part of the solution while the tilde (~) will refer to the rotational part. Following Flandro,[33] the rotational and irrotational pressure and velocity components can be derived directly from Eqs. (2) and (3). One obtains

$$\hat{p}^{(1)} = e^{-ikt}\cos(k_m z) + O(M_b), \tag{5}$$

$$\hat{\mathbf{u}}^{(1)} = ie^{-ikt}\sin(k_m z)\mathbf{e}_z + O(M_b), \tag{6}$$

for the irrotational field, and

$$\tilde{p}^{(1)} = iM_b e^{-ikt}\sin(2x)e^{(\phi+i\psi)\left(\frac{1}{2}\pi z\right)}\sin[\sin(x)k_m z] + O(M_b^2), \tag{7}$$

$$\tilde{\mathbf{u}}^{(1)} = ie^{-ikt}rU_r e^{(\phi+i\psi)}\sin[\sin(x)k_m z]\mathbf{e}_z + O(M_b), \tag{8}$$

for the rotational field. In the above, k_m represents the dimensionless wave number which, for closed-end boundaries, is

given by $k_m = m\pi R/L = m\pi/l$, where m is the mode shape number and $l \equiv L/R$ is the aspect ratio for the motor.[14]

The imaginary part of the exponential argument in Eq. (7), namely,

$$\psi(r) = -[k_m/(\pi M_b)]\ln\tan\left(\tfrac{1}{2}x\right), \tag{9}$$

controls the wavelength and spatial frequency of the shear wave. The real argument, $\phi(r)$, is responsible for the viscous decay of shear waves. It is given by[22]

$$\phi(r) = \frac{\xi}{\pi^2}\left[1 - \frac{1}{\sin(x)} - x\frac{\cos(x)}{\sin^2(x)} + I(x) - I\left(\frac{1}{2}\pi\right)\right], \tag{10}$$

$$I(x) = x + \tfrac{1}{18}x^3 + \tfrac{7}{1800}x^5 + \tfrac{31}{105\,840}x^7 + \cdots, \tag{11}$$

where S and ξ are dimensionless scaling factors related via

$$S \equiv \frac{k_m}{M_b} = \frac{m}{l}\frac{\pi}{M_b}, \quad \xi \equiv \frac{k_m^2\delta^2}{M_b^3} = \frac{S^2\delta^2}{M_b} = \frac{m^2}{l^2}\frac{\pi^2\delta^2}{M_b^3}. \tag{12}$$

While S represents the Strouhal number, ξ is a viscous parameter whose reciprocal has been coined the penetration number due to the role that it commands in controlling the penetration depth of the so-called acoustic boundary layer.[18–22] For constant $\delta = \sqrt{\nu/(a_0 R)} = \xi^{1/2}M_b^{3/2}l/(m\pi)$ and surface Mach number, S and ξ decrease in more elongated motors. Their physical variation is illustrated in Fig. 2 over a range of chamber lengths.

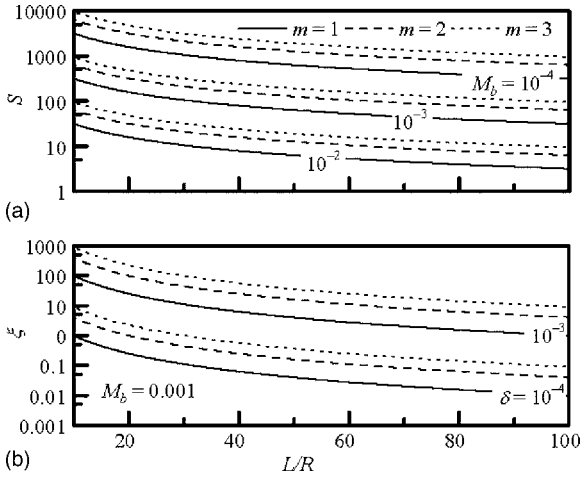

FIG. 2. Variation of (a) the Strouhal number and (b) ξ over a range of motor aspect ratios and the first three acoustic oscillation modes.

A. Unsteady energy

Following the classical acoustics approach,[43] one defines the unsteady energy density to be

$$e = \tfrac{1}{2}(\hat{p}^2 + \mathbf{u}\cdot\mathbf{u}). \tag{13}$$

Subsequently, the time-averaged energy residing in the chamber can be calculated from

$$E = \iiint_V \langle e\rangle dV = \tfrac{1}{2}\iiint_V \left\langle \hat{p}^2 + \mathbf{u}\cdot\mathbf{u}\right\rangle dV. \tag{14}$$

Note that triangular brackets require time averaging of the enclosed function. This is accomplished via

$$\langle A\rangle = \frac{1}{2\pi}k_m e^{\alpha_m t}\int_0^{2\pi/k_m} A e^{-\alpha_m t}dt. \tag{15}$$

The evolution of the system energy is then determined by taking the time rate of change of the total internal energy. Using $\boldsymbol{\Omega} = \nabla\times\mathbf{U}$ and $\boldsymbol{\omega} = \nabla\times\tilde{\mathbf{u}}$ to represent mean and unsteady vorticities, one finds

$$\begin{aligned}\frac{dE}{dt} = \iiint_V \Big\langle & \overbrace{-\nabla\cdot(\hat{p}\hat{\mathbf{u}}) - \tfrac{1}{2}M_b(\mathbf{U}\cdot\nabla\hat{p}^2) - M_b[\hat{\mathbf{u}}\cdot\nabla(\mathbf{U}\cdot\hat{\mathbf{u}})]}^{\text{irrotational}} \\ & + \tfrac{4}{3}\delta^2\hat{\mathbf{u}}\cdot\nabla(\nabla\cdot\hat{\mathbf{u}}) + M_b[\hat{\mathbf{u}}\cdot(\hat{\mathbf{u}}\times\boldsymbol{\Omega}) + \hat{\mathbf{u}}\cdot(\mathbf{U}\times\boldsymbol{\omega})] \\ & \overbrace{-\tilde{\mathbf{u}}\cdot\nabla\hat{p} - M_b\begin{bmatrix}\tilde{\mathbf{u}}\cdot\nabla(\mathbf{U}\cdot\hat{\mathbf{u}} + \hat{\mathbf{u}}\cdot\nabla(\mathbf{U}\cdot\tilde{\mathbf{u}}) + \tilde{\mathbf{u}}\cdot\nabla(\mathbf{U}\cdot\tilde{\mathbf{u}}) \\ -\tilde{\mathbf{u}}\cdot(\mathbf{U}\times\boldsymbol{\omega}) - \tilde{\mathbf{u}}\cdot(\tilde{\mathbf{u}}\times\boldsymbol{\Omega})\end{bmatrix}}^{\text{rotational}} \\ & + \tfrac{4}{3}\delta^2\tilde{\mathbf{u}}\cdot\nabla(\nabla\cdot\hat{\mathbf{u}}) - \delta^2[\hat{\mathbf{u}}\cdot(\nabla\times\boldsymbol{\omega}) + \tilde{\mathbf{u}}\cdot(\nabla\times\boldsymbol{\omega})] - \hat{\mathbf{u}}\cdot\nabla\tilde{p} - \tilde{\mathbf{u}}\cdot\nabla\tilde{p}\Big\rangle dV.\end{aligned} \tag{16}$$

After careful simplifications several quantities cancel from Eq. (16). The remaining terms control the rate at which the system energy changes. Based on this information, one can estimate the growth or decay rate for a given motor configuration.

B. On the unsteady rotational contribution

The object of the current calculations is to analyze the stability of the system of waves consisting of the irrotational (acoustic) motions with the required rotational components. The latter must be treated as an integral part of the gas

fluctuations in order for the proper boundary conditions to be accommodated. It is incorrect to treat the growth of the waves in the chamber as an acoustic problem with weak perturbations from the vorticity (and other physical processes). Both rotational and acoustic waves must exist at the same order in order to satisfy the no slip condition. Their combined energies must also be included to determine wave growth.

The separation of the gas motions into two parts is merely a convenient way to simplify the computations. In an oscillating flow with gas motions parallel to a surface, especially, a surface with mass flux, the wave system cannot be described in terms of acoustic waves only. We have, in fact, compressible rotational waves. In experimental data from rocket tests, there is little evidence of this because only pressure measurements can be made and these heavily reflect the acoustic component only (since the pseudopressure is secondary). The cold flow simulations by Avalon and Comas,[44] and Brown, Dunlap, Young, and Waugh[45] support this concept. The composite (acoustic and shear) waves are clearly present in the data with sidewall mass injection and parallel wave motions. The data by Center for Simulation of Advanced Rockets (CSAR) and Office National d'Etudes et de Recherches Aerospatiales (ONERA) scientists also corroborate our analysis. It is important to realize that the effective amplitude of *both* components must grow or decay at precisely the same rate. They are integral parts of the unsteady field, and must be treated as such in the stability calculations. Our approach is based on the use of their combined energies.

In an energy representation of the stability problem, we believe it is necessary that all of the unsteady energy be properly accounted for. Historically, the dismissal of the rotational energy was made in problems that did not exhibit cross-flow (cross-steamwise or transverse flow across porous surfaces), and in which rotational effects did not penetrate deep into the chamber. These were problems in which rotational effects were indeed negligible or confined to very thin layers—thus justifying the purely acoustic representation. In our problem, the rotational layer is quite large; in fact, most studies published in the late 1990s predict large unsteady rotational depths: the unsteady rotational region occupies nearly 80% of the chamber volume (or more).[19] In view of this, the energy associated with the unsteady rotational waves appears to be an appreciable component that must not be discounted.

C. Stability variables

In order to assess the time evolution of the total system energy, one can put

$$k = k_m + (\omega_m + i\alpha_m) + O(M_b^2), \tag{17}$$

where k_m is the wave number for the unperturbed acoustic mode m. For a system dominated by longitudinal oscillation modes, a single integer m will suffice in identifying the mode under consideration. Following the conventional energy-balance procedure, the small frequency correction ω_m is not evaluated. The real parts of Eqs. (5), (6), and (8) yield

$$\hat{p} = \hat{p}_m \exp(\alpha_m t)\cos(k_m t), \tag{18}$$

$$\hat{\mathbf{u}} = \hat{\mathbf{u}}_m \exp(\alpha_m t)\sin(k_m t), \tag{19}$$

$$\tilde{\mathbf{u}} = \exp(\alpha_m t)\left[\tilde{\mathbf{u}}_m^r \cos(k_m t) + \tilde{\mathbf{u}}_m^i \sin(k_m t)\right], \tag{20}$$

where the superscripts (r,i) stand for the real and imaginary parts; in like fashion, one finds

$$\hat{p}_m = \cos(k_m z), \tag{21}$$

$$\hat{\mathbf{u}}_m = \sin(k_m z)\mathbf{e}_z, \tag{22}$$

$$\tilde{\mathrm{u}}_m^r = \sin(x)\exp(\phi)\sin(\psi)\sin[\sin(x)k_m z]\mathbf{e}_z, \tag{23}$$

$$\tilde{\mathrm{u}}_m^i = -\sin(x)\exp(\phi)\cos(\psi)\sin[\sin(x)k_m z]\mathbf{e}_z. \tag{24}$$

The acoustic pressure and velocity mode shapes are related by $\hat{\mathbf{u}}_m = -\nabla \hat{p}_m / k_m$.

D. Unsteady energy normalization form

These expressions can be inserted into Eq. (14), time averaged, and time differentiated. At the outset, one can write

$$\frac{dE}{dt} = \alpha_m^{(1)} \exp(2\alpha_m t) E_m^2, \tag{25}$$

where the acoustic energy normalization function emerges as

$$E_m^2 = \tfrac{1}{2}\iiint [(p'_m)^2 + \hat{\mathbf{u}}_m \cdot \hat{\mathbf{u}}_m + 2\hat{\mathbf{u}}_m \cdot \tilde{\mathbf{u}}_m^i + \tilde{\mathbf{u}}_m^r \cdot \tilde{\mathbf{u}}_m^r + \tilde{\mathbf{u}}_m^i \cdot \tilde{\mathbf{u}}_m^i] dV. \tag{26}$$

When the entire volume integral of Eq. (26) is carried out for the axial mode case, one finds

$$E_m^2 = \tfrac{5}{8}\pi L/R = \tfrac{5}{8}\pi l. \tag{27}$$

This value is valid for an internal burning motor of length L and effective radius R.

III. ACOUSTIC GROWTH RATE CALCULATIONS

The linear system growth rate $\alpha_m^{(1)}$ for a given oscillation mode consists of the linear superposition of several volume integrals that can be segregated from Eq. (16). Writing

$$\alpha_m^{(1)} = \alpha_1 + \alpha_2 + \alpha_3 + \cdots = \sum_{i=1}^{N} \alpha_i, \tag{28}$$

these integrals can be carried out individually, or in combination, depending on their general form. Naturally, the composite growth rate of the system will be a linear sum of these factors. The main contribution of this analysis lies in the presentation of these corrections to higher order of accuracy, thus enabling us to propose stability criteria and critical parameters that delineate the stability regions. In the process, we derive the unsteady nozzle loss (not considered previously), prove that $\alpha_3 = 0$ for an arbitrary profile, and demonstrate that the flow turning loss α_4 and the pseudorotational gain α_9 are offset by the rotational flow gain α_5 and the unsteady nozzle loss α_{10}, respectively.

A. First factor: Extended pressure coupling

The first correction factor combines the first three irrotational integrals representing pressure coupling and nozzle damping due to the acoustic energy carried out by the mean flow,

$$\alpha_1 = \frac{1}{\exp(2\alpha_m t)E_m^2}\int\int\int_V \left\langle -\nabla\cdot\left[\hat{p}\hat{\mathbf{u}} + \frac{1}{2}M_b\mathbf{U}(\hat{p})^2\right] - M_b[\hat{\mathbf{u}}\cdot\nabla(\mathbf{U}\cdot\hat{\mathbf{u}})]\right\rangle dV. \tag{29}$$

Using Gauss's theorem, one transforms the integrand with the divergence operator into a simpler surface integral. One gets

$$\alpha_1 = \underbrace{-\frac{1}{\exp(2\alpha_m t)E_m^2}\int\int_S \left\langle \mathbf{n}\cdot\left[\hat{p}\hat{\mathbf{u}} + \tfrac{1}{2}M_b\mathbf{U}\hat{p}^2\right]\right\rangle dS}_{\mathrm{I}} + \underbrace{\frac{1}{\exp(2\alpha_M t)E_m^2}\int\int\int_V \langle -M_b[\hat{\mathbf{u}}\cdot\nabla(\mathbf{U}\cdot\hat{\mathbf{u}})]\rangle dV}_{\mathrm{II}}. \tag{30}$$

At this point, vector projections along the outward pointing unit normal vector $\mathbf{n}$ must be carefully evaluated along different sections of the enclosure delineating the idealized rocket motor chamber. These include: First, along the burning surface,

$$\mathbf{n}\cdot\hat{\mathbf{u}} = -M_b A_b^{(r)}\hat{p}, \quad \mathbf{n}\cdot\mathbf{U} = -1. \tag{31}$$

Second, along the inert surface,

$$\mathbf{n}\cdot\hat{\mathbf{u}} = -M_b A_S^{(r)}\hat{p}, \quad \mathbf{n}\cdot\mathbf{U} = 0, \tag{32}$$

with $A_S^{(r)}$ being the inert surface admittance. Thirdly, along the nozzle entrance plane,

$$\mathbf{n}\cdot\hat{\mathbf{u}} = M_b A_N^{(r)}\hat{p}, \quad \mathbf{n}\cdot\mathbf{U} = U_N, \tag{33}$$

where $A_N^{(r)}$ is the nozzle admittance and U_N is the mean axial velocity crossing the nozzle entrance plane at $z=l$. A new term will be later introduced in Sec. III J to account for the unsteady axial energy crossing this plane.

Assuming that $A_S^{(r)}$ is small compared to other terms, Eqs. (31)–(33) can be substituted back into Eq. (30). The first integral becomes

$$\mathrm{I} = \frac{-1}{\exp(2\alpha_m t)E_m^2}\int\int_S \left\langle -M_b A_b^{(r)}\hat{p}^2 + M_b A_N^{(r)}\hat{p}^2 + \frac{1}{2}M_b\hat{p}^2(-1+U_N)\right\rangle dS. \tag{34}$$

Grouping and rearranging, Eq. (34) simplifies into

$$\mathrm{I} = \frac{-M_b}{\exp(2\alpha_m t)E_m^2}\int\int_S \left\langle \hat{p}^2\left[-A_b^{(r)} - \frac{1}{2}\right] + \hat{p}^2\left[A_N^{(r)} + \frac{1}{2}U_N\right]\right\rangle dS. \tag{35}$$

At this juncture, one inserts the value of $\hat{p}^2$ and carries out the time averaging; this leads to

$$\mathrm{I} = \frac{M_b}{2E_m^2}\left(\int\int_{S_b}\left\{\cos^2(k_m z)\left[A_b^{(r)} + \frac{1}{2}\right]\right\}dS - \int\int_{S_N}\left\{\cos^2(k_m z)\left[A_N^{(r)} + \frac{1}{2}U_N\right]\right\}dS\right). \tag{36}$$

In much the same way, the second integral of Eq. (30) can be written as

$$\mathrm{II} = \frac{-1}{\exp(2\alpha_m t)E_m^2}\int\int\int_V \langle M_b[\hat{\mathbf{u}}\cdot\nabla(\mathbf{U}\cdot\hat{\mathbf{u}})]\rangle dV = \frac{M_b}{\exp(2\alpha_m t)E_m^2}\int\int\int_V \langle(\mathbf{U}\cdot\hat{\mathbf{u}})\nabla\cdot\hat{\mathbf{u}}\rangle dV, \tag{37}$$

where the divergence of the mean flow vector has been set equal to zero. The time average can now be readily evaluated. One gets

$$\mathrm{II} = -\frac{1}{2}M_b E_m^{-2}\int\int_S\left(\frac{1}{2}\mathbf{n}\cdot\mathbf{U}\hat{p}_m^2\right)dS = \frac{1}{2}M_b E_m^{-2}\left(\int\int_{S_b}\frac{1}{2}\hat{p}_m^2 dS - \int\int_{S_N}\frac{1}{2}U_N\hat{p}_m^2 dS\right). \tag{38}$$

Combining Eqs. (38) and (36), Eq. (29) becomes

$$\alpha_1 = \frac{1}{2}M_b E_m^{-2}\left\{\int\int_{S_b}\frac{1}{2}\cos^2(k_m z)dS - \int\int_{S_N}\left[\frac{1}{2}U_N\cos^2(k_m z)\right]dS\right\} + \frac{1}{2}M_b E_m^{-2}\left(\int\int_{S_b}\left\{\cos^2(k_m z)\left[A_b^{(r)} + \frac{1}{2}\right]\right\}dS + \int\int_{S_N}\left\{\cos^2(k_m z)\left[-A_N^{(r)} - \frac{1}{2}U_N\right]\right\}dS\right). \tag{39}$$

Collecting same type integrals, one obtains, at length,

$$\alpha_1 = \frac{1}{2}M_b E_m^{-2}\int\int_{S_b}\cos^2(k_m z)\left[A_b^{(r)} + 1\right]dS - \frac{1}{2}M_b E_m^{-2}\int\int_{S_N}\cos^2(k_m z)\left[A_N^{(r)} + U_N\right]dS. \tag{40}$$

By applying a mass balance to an internal burning solid rocket motor, one obtains $2\pi RLV_b = \pi R^2 U_N^*$ or $U_N = 2l$. Then using $A_N^{(r)} = (\gamma-1)l$, Eq. (40) can be simplified into

$$\alpha_1 = \tfrac{1}{2}\pi l M_b E_m^{-2}\{[A_b^{(r)}+1][1+\sin(2k_m l)/(2k_m l)] - \cos^2(k_m l)(\gamma+1)\}. \tag{41}$$

It should be noted that, by virtue of $k_m = m\pi/l$,

$$\begin{cases} \sin(2k_m l) = \sin(2m\pi) = 0 \\ \cos(k_m l) = \cos(m\pi) = \pm 1 \end{cases}, \ \forall\, m \in \mathbb{N}. \tag{42}$$

The first growth rate factor becomes

$$\alpha_1 = \tfrac{1}{2}\pi l M_b E_m^{-2}[A_b^{(r)} - \gamma] = \tfrac{4}{5} M_b[A_b^{(r)} - \gamma]. \tag{43}$$

B. Second factor: Dilatational energy correction

The fourth irrotational term in Eq. (16) leads to

$$\alpha_2 = \frac{1}{E_m^2 \exp(2\alpha_m t)} \int\int\int_V \left\langle \frac{4}{3}\delta^2 \hat{\mathbf{u}} \cdot \nabla(\nabla \cdot \hat{\mathbf{u}}) \right\rangle dV. \tag{44}$$

Starting with the definition of acoustic velocity and pressure, one can put

$$\nabla \cdot \hat{\mathbf{u}} = \exp(\alpha_m t)\sin(k_m t)\nabla \cdot (-\nabla \hat{p}_m/k_m) = k_m \exp(\alpha_m t)\sin(k_m t)\cos(k_m z), \tag{45}$$

and so

$$\nabla(\nabla \cdot \hat{\mathbf{u}}) = \nabla[k_m \exp(\alpha_m t)\sin(k_m t)\cos(k_m z)] = -k_m^2 \exp(\alpha_m t)\sin(k_m t)\sin(k_m z)\mathbf{e}_z, \tag{46}$$

turning α_2 into

$$\alpha_2 = -\tfrac{4}{3}k_m^2 \delta^2 E_m^{-2} \int\int\int_V \langle \sin^2(k_m z)\sin^2(k_m t)\rangle dV. \tag{47}$$

After time averaging, Eq. (47) reduces to

$$\alpha_2 = -\tfrac{2}{3}k_m^{-2} \delta^2 E_m^{-2} \int\int\int_V \sin^2(k_m z) dV. \tag{48}$$

Using $dV = r dz dr d\theta$, the triple integral can be expressed as

$$\alpha_2 = -\frac{2}{3}k_m^2 \delta^2 E_m^{-2} \int_0^{2\pi}\int_0^1\int_0^{L/R} \sin^2(k_m z) r dz dr d\theta = -\frac{1}{3}\pi k_m^2 l \delta^2 E_m^{-2}[1-\sin(2k_m l)/(2k_m l)] = -\frac{1}{3}\pi k_m^2 l \delta^2 E_m^{-2} = -\frac{8}{15}\xi M_b^3. \tag{49}$$

C. Third factor: Acoustic mean flow correction

The fifth term in Eq. (16) can be evaluated from

$$\alpha_3 = \frac{1}{E_m^2 \exp(2\alpha_m t)} \int\int\int_V \langle M_b\{\hat{\mathbf{u}} \cdot (\hat{\mathbf{u}} \times \boldsymbol{\Omega})\}\rangle dV. \tag{50}$$

Being the mean flow vorticity, $\boldsymbol{\Omega}$ can be approximated from

$$\boldsymbol{\Omega} = \Omega \hat{\mathbf{e}}_\theta = \pi^2 r z \sin(x)\mathbf{e}_\theta, \tag{51}$$

and so

$$\hat{\mathbf{u}} \times \boldsymbol{\Omega} = -\Omega \hat{u}_z \mathbf{e}_r + \Omega \hat{u}_r \mathbf{e}_z. \tag{52}$$

Therefore, at any order,

$$\hat{\mathbf{u}} \cdot (\hat{\mathbf{u}} \times \boldsymbol{\Omega}) = (\hat{u}_r \hat{\mathbf{e}}_r + \hat{u}_z \hat{\mathbf{e}}_z) \cdot (-\Omega \hat{u}_z \hat{\mathbf{e}}_r + \Omega \hat{u}_r \hat{\mathbf{e}}_z) = -\hat{u}_r \Omega \hat{u}_z + \hat{u}_z \Omega \hat{u}_r = 0. \tag{53}$$

Evidently, this vector identity causes α_3 to vanish. Upon closer examination, it may be useful to note that α_3 vanishes for an arbitrary profile because $\hat{\mathbf{u}}$ and $\hat{\mathbf{u}} \times \boldsymbol{\Omega}$ are always perpendicular.

D. Fourth factor: Flow turning correction

The sixth term in Eq. (16) is a function of the unsteady vorticity. Nonetheless, this term has often been dubbed the flow turning loss in the irrotational stability formulation. It is kept among the irrotational terms to reflect its presence in the classic formulation. Starting with

$$\alpha_4 = \frac{E_m^{-2}}{\exp(2\alpha_m t)} \int\int\int_V \langle M_b \hat{\mathbf{u}} \cdot (\mathbf{U} \times \boldsymbol{\omega})\rangle dV = \frac{-M_b E_m^{-2}}{k_m \exp(2\alpha_m t)} \int\int\int_V \langle \nabla \hat{p} \tan(k_m t) \cdot (\mathbf{U} \times \boldsymbol{\omega})\rangle dV, \tag{54}$$

one recalls that $\partial \tilde{u}_r/\partial z = O(M_b{}^2)$ so that $\boldsymbol{\omega} = \nabla \times \tilde{\mathbf{u}} = -(\partial \tilde{u}_z/\partial r)\mathbf{e}_\theta$. Using the definition of $\tilde{u}_z$, the unsteady vorticity is expressible by

$$\boldsymbol{\omega} = -\exp(\alpha_m t)\left[\frac{\partial \tilde{u}_m^r}{\partial r}\cos(k_m t) + \frac{\partial \tilde{u}_m^i}{\partial r}\sin(k_m t)\right]\mathbf{e}_\theta. \tag{55}$$

Using the fact that $\mathbf{U} \times \boldsymbol{\omega} = (-U_z \omega)\mathbf{e}_r + (U_r \omega)\mathbf{e}_z$, one can rewrite α_4 as

$$\alpha_4 = \frac{M_b E_m^{-2}}{\exp(2\alpha_m t)} \int\int\int_V \langle [\sin(k_m z)\exp(\alpha_m t) \times \sin(k_m t)]\mathbf{e}_z \cdot (-U_z \omega \mathbf{e}_r + U_r \omega \mathbf{e}_z)\rangle dV, \tag{56}$$

hence,

$$\alpha_4 = \frac{M_b E_m^{-2}}{\exp(2\alpha_m t)} \int\int\int_V \langle \sin(k_m z)\exp(\alpha_m t)\sin(k_m t) U_r \omega\rangle dV \tag{57}$$

or

$$\alpha_4 = \frac{-M_b E_m^{-2}}{e^{2\alpha_m t}} \int\int\int_V \left\langle U_r \sin(k_m z)\exp(2\alpha_m t)\sin(k_m t) \times \left[\frac{\partial \tilde{u}_m^r}{\partial r}\cos(k_m t) + \frac{\partial \tilde{u}_m^i}{\partial r}\sin(k_m t)\right]\right\rangle dV. \tag{58}$$

Equation (58) can, in turn, be partitioned into two terms such as

$$\alpha_4 = \frac{-M_b}{E_m^2 e^{2\alpha_m t}} \iiint_V \Bigg\langle \underbrace{\tfrac{1}{2} U_r \sin(k_m z)\exp(2\alpha_m t)\sin(2k_m t)\frac{\partial \tilde{u}_m^r}{\partial r}}_{\mathrm{I}} + \underbrace{U_r \sin(k_m z)\exp(2\alpha_m t)\sin^2(k_m t)\frac{\partial \tilde{u}_m^i}{\partial r}}_{\mathrm{II}} \Bigg\rangle dV. \tag{59}$$

Forthwith, term I gives

$$\mathrm{I} = \left\langle \frac{1}{2} U_r \sin(k_m z)\exp(2\alpha_m t)\sin(2k_m t)\frac{\partial \tilde{u}_m^r}{\partial r} \right\rangle = \frac{k_m}{4\pi}\exp(2\alpha_m t) U_r \sin(k_m z)\frac{\partial \tilde{u}_m^r}{\partial r}\int_0^{2\pi/k_m} \sin(2k_m t)dt = 0, \tag{60}$$

being vanishingly small, one is left with term II; this can be calculated from

$$\mathrm{II} = \left\langle U_r \sin(k_m z)\exp(2\alpha_m t)\sin^2(k_m t)\frac{\partial \tilde{u}_m^i}{\partial r} \right\rangle = \frac{k_m}{2\pi}\exp(2\alpha_m t) U_r \sin(k_m z)\frac{\partial \tilde{u}_m^i}{\partial r}\int_0^{2\pi/k_m} \sin^2(k_m t)dt = \frac{1}{2}\exp(2\alpha_m t) U_r \sin(k_m z)\frac{\partial \tilde{u}_m^i}{\partial r}. \tag{61}$$

Combining, Eq. (58) becomes

$$\alpha_4 = \frac{-M_b}{2E_m^2}\int\int\int_V U_r \sin(k_m z)\frac{\partial \tilde{u}_m^i}{\partial r} dV, \tag{62}$$

where the derivative must be evaluated from

$$\frac{\partial \tilde{u}_m^i}{\partial r} = -\sin x \exp\phi \frac{\partial(\cos\psi)}{\partial r}\sin(k_m z \sin x) + \cdots. \tag{63}$$

Only the leading term in this derivative is shown, being one order of magnitude larger than other quantities resulting from chain-rule differentiation. The dominance of this term is due to the derivative of ψ being proportional to the inverse of the mean flow Mach number. At the outset, one identifies that

$$\frac{\partial \tilde{u}_m^i}{\partial r} \approx \frac{k_m}{M_b U_r}\sin(x)\exp(\phi)\sin(\psi)\sin[\sin(x)k_m z]. \tag{64}$$

Inserting Eq. (64) into Eq. (62) gives

$$\alpha_4 = -\frac{1}{2}k_m E_m^{-2}\int_0^{2\pi} d\theta \int_0^{L/R}\int_0^1 r \sin(x)\exp(\phi)\sin(\psi) \times \sin(k_m z \sin x)\sin(k_m z) dr dz. \tag{65}$$

Subsequently, expanding r as $1-y$, one gets

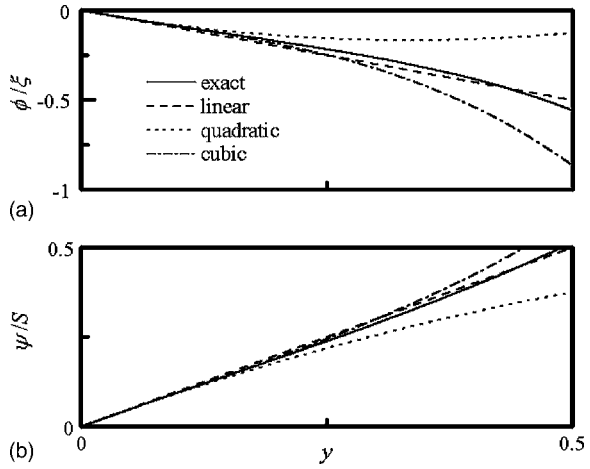

FIG. 3. Comparison of exact representations and polynomial approximations for (a) ϕ and (b) ψ. In both cases, the leading-order linear approximation outperforms the higher-order polynomials in the domain above the wall where most meaningful interactions take place.

$$\alpha_4 = -\pi k_m E_m^{-2}\int_0^1\int_0^1 (1-y)\sin\left[\frac{1}{2}\pi(1-2y+y^2)\right] \times \sin(k_m z)\sin\left\{\sin\left[\frac{1}{2}\pi(1-2y+y^2)\right]k_m z\right\} \times \sin(\psi)\exp(\phi) dz dy. \tag{66}$$

The first integral with respect to z renders

$$\alpha_4 = -\pi k_m E_m^{-2}\int_0^1 (1-y)\sin\left[\frac{1}{2}\pi(1-2y+y^2)\right] \times \sin(\psi)\exp(\phi) \times \left[\frac{\sin\left(k_m l\left\{1-\sin\left[\frac{1}{2}\pi(1-2y+y^2)\right]\right\}\right)}{2k_m\left\{1-\sin\left[\frac{1}{2}\pi(1-2y+y^2)\right]\right\}} - \frac{\sin\left(k_m l\left\{1+\sin\left[\frac{1}{2}\pi(1-2y+y^2)\right]\right\}\right)}{2k_m\left\{1+\sin\left[\frac{1}{2}\pi(1-2y+y^2)\right]\right\}}\right] dy. \tag{67}$$

At this juncture, one must carefully examine the spatial behavior of each term in Eq. (67). One finds that linearization of certain terms will be appropriate prior to integration. To start, both ψ and ϕ must be fully expanded using MacLaurin series; one finds

$$\psi = (k_m/M_b)\left(y - \tfrac{1}{2}y^2 + \tfrac{1}{6}\pi^2 y^3 - \tfrac{1}{4}\pi^2 y^4 + \cdots\right), \tag{68}$$

$$\phi = -\xi\left(y + \tfrac{3}{2}y^2 - 5.9348y^3 + 15.0544y^4 + \cdots\right). \tag{69}$$

It can be easily shown by plotting these functions (see Fig. 3) that the leading-order representations for ψ and ϕ lead to very good approximations. Interestingly, these one-term approximations outperform higher-order polynomial representations except near the core; the deterioration of the one-term approximations near the core is immaterial: boundary-driven rotational effects are significant near the walls only. Consequently, one can put

$$\sin(\psi) = \sin(k_m y/M_b) + O(y^2), \tag{70}$$

$$\exp(\phi) = \exp(-\xi y) + O(y^2). \tag{71}$$

To be consistent, all (but the last two terms) remaining in Eq. (67) must be linearized to the order of y^2. The resulting expression for α_4 becomes

$$\alpha_4 = -\frac{1}{2}\pi k_m E_m^{-2}\int_0^1 \sin(k_m y/M_b)\exp(-\xi y) \times\left\{ l - \frac{1}{2}\sin(2k_m l)/k_m - y\left[l - \frac{1}{2}\sin(2k_m l)/k_m \right]\right\} dy. \tag{72}$$

At first glance, the exact integral of Eq. (72) appears to be intractable. Nonetheless, an inviscid result can be easily extracted by suppressing the viscous parameter ξ. The inviscid form of α_4 turns out to be

$$\alpha_4^0 = -\tfrac{1}{2}\pi l M_b E_m^{-2}[1 - \sin(2k_m l)/(2k_m l)]. \tag{73}$$

Knowing that the exact integral must match the inviscid solution in the limit as $\xi \to 0$, we use inductance and reevaluate Eq. (72); at the outset, we obtain

$$\begin{aligned}\alpha_4 &= -\tfrac{1}{2}\pi l M_b E_m^{-2}[1 - \sin(2k_m l)/(2k_m l)](1 + M_b^2\xi^2/k_m^2)^{-1}\\ &= -\tfrac{1}{2}\pi l M_b E_m^{-2}(1 + M_b^2\xi^2/k_m^2)^{-1}\\ &= -\tfrac{4}{5}M_b(1 + \pi^{-2}M_b^2\xi^2 l^2 m^{-2})^{-1}.\end{aligned} \tag{74}$$

This expression approximates Eq. (62) to within a few percent over a wide range of M_b, ξ, l, and m.

E. Fifth factor: Rotational flow correction

The integrals considered thus far are those that have been traditionally accepted in stability assessments. As emphasized by Flandro and Majdalani,[33] consistent retention of unsteady rotational terms gives way to several additional integrals. The first rotational flow stability integral in Eq. (16) has the form

$$\alpha_5 = \frac{1}{E_m^2\exp(2\alpha_m t)}\int\int\int_V \langle -\tilde{\mathbf{u}}\cdot\nabla\hat{p}\rangle dV. \tag{75}$$

The integrand stems from

$$-\tilde{\mathbf{u}}\cdot\nabla\hat{p} = k_m\sin(k_m z)\exp(2\alpha_m t) \times\left[\tilde{u}_m^r\cos^2(k_m t) + \tilde{u}_m^i\sin(k_m t)\cos(k_m t)\right], \tag{76}$$

so that α_5 can now be written as

$$\alpha_5 = \frac{k_m}{E_m^2\exp(2\alpha_m t)}\int\int\int_V \exp(2\alpha_m t) \times\left\langle\left[\sin(k_m z)\tilde{u}_m^r\cos^2(k_m t) + \sin(k_m z)\tilde{u}_m^i\sin(k_m t)\cos(k_m t)\right]\right\rangle dV. \tag{77}$$

Carrying out the time average of the last expression, one gets

$$\alpha_5 = \frac{k_m}{2E_m^2}\int\int\int_V \sin(x)\exp(\phi)\sin(\psi)\sin[k_m z\sin(x)] \times\sin(k_m z)dV. \tag{78}$$

At this point, the volume integral can be expanded into

$$\alpha_5 = \frac{1}{2}k_m E_m^{-2}\int_0^{2\pi}d\theta\int_0^1\int_0^1 r\sin(x)\exp(\phi)\sin(\psi) \times\sin[k_m z\sin(x)]\sin(k_m z)dz dr. \tag{79}$$

This expression is the negative of Eq. (65). Following the same lines as before, α_5 becomes

$$\alpha_5 = \tfrac{4}{5}M_b(1 + \pi^{-2}M_b^2\xi^2 l^2 m^{-2})^{-1}. \tag{80}$$

Except for having an opposite sign, this expression is identical to the flow turning integral ($\alpha_5 = -\alpha_4$). The flow turning loss is hence phased out due to the rotational flow correction even when higher-order approximations are used. At first glance, this result seems paradoxical. Upon further examination, however, it appears to be in total accord with Van Moorhem's formal work[34] in which he proves that flow turning, albeit quintessential to one-dimensional models of porous chambers, will disappear in two- and three-dimensional settings.

It is now necessary to tackle the remaining terms in Eq. (16). Some of them do not contribute to the system energy and are carefully described by Flandro and Majdalani.[33] Specifically, the second, third, and sixth rotational integrals in Eq. (16) can be shown to be of second order in the Mach number.

F. Sixth factor: Inviscid vortical correction

The fifth rotational term in Eq. (16) can be written as

$$\alpha_6 = \frac{1}{E_m^2\exp(2\alpha_m t)}\int\int\int_V \left\langle M_b\tilde{\mathbf{u}}\cdot(\mathbf{U}\times\boldsymbol{\omega})\right\rangle dV. \tag{81}$$

This can be further simplified into

$$\alpha_6 = \frac{M_b}{E_m^2\exp(2\alpha_m t)}\int\int\int_V \left\langle\exp(\alpha_m t)\left[\tilde{u}_m^r\cos(k_m t) + \tilde{u}_m^i\sin(k_m t)\right]\mathbf{e}_z\cdot[-U_z\omega\mathbf{e}_r + U_r\omega\mathbf{e}_z]\right\rangle dV. \tag{82}$$

Direct expansion gives

$$\alpha_6 = \frac{-M_b}{E_m^2\exp(2\alpha_m t)}\int\int\int_V \left\langle U_r\exp(2\alpha_m t) \times\left[(\partial\tilde{u}_m^r/\partial r)\cos(k_m t) + (\partial\tilde{u}_m^i/\partial r)\sin(k_m t)\right] \times\left[\tilde{u}_m^r\cos(k_m t) + \tilde{u}_m^i\sin(k_m t)\right]\right\rangle dV. \tag{83}$$

After carrying out the time averaging operation, one is left with

$$\alpha_6 = \frac{-M_b}{2E_m^2}\int\int\int_V U_r\left(\frac{\partial\tilde{u}_m^r}{\partial r}u_m^r + \frac{\partial\tilde{u}_m^i}{\partial r}u_m^i\right)dV, \tag{84}$$

which reduces to

$$\alpha_6 = \frac{-M_b}{4E_m^2}\int\int\int_V U_r\left[\frac{\partial}{\partial r}\left(\tilde{u}_m^{r\,2}+\tilde{u}_m^{i\,2}\right)\right]dV. \tag{85}$$

By substituting the values of $\tilde{u}_m^r$ and $\tilde{u}_m^i$ into Eq. (85), one reaps

$$\begin{aligned}\alpha_6 = \frac{-M_b}{4E_m^2}\int\int\int_V U_r\{&\sin^2(x)\exp(2\phi)\sin^2(\psi)\\ &\times\sin^2[k_m z\,\sin(x)]+\sin^2(x)\exp(2\phi)\cos^2(\psi)\\ &\times\sin^2[k_m z\,\sin(x)]\}_r dV,\end{aligned} \tag{86}$$

where the subscript denotes partial differentiation with respect to r. Since $\sin^2(\psi)+\cos^2(\psi)=1$, Eq. (86) collapses into

$$\alpha_6 = \frac{-M_b}{4E_m^2}\int\int\int_V U_r\{\sin^2(x)\exp(2\phi)\sin^2[k_m z\,\sin(x)]\}_r dV. \tag{87}$$

As usual, the independent variable is switched such that

$$\begin{aligned}\alpha_6 = \frac{-M_b}{4E_m^2}\int\int\int_V &(1-y)^{-1}\sin\left[\frac{1}{2}\pi(1-2y+y^2)\right]\\ &\times\left(\sin^2\left[\frac{1}{2}\pi(1-2y+y^2)\right]\exp(2\phi)\right.\\ &\left.\times\sin^2\left\{k_m z\,\sin\left[\frac{1}{2}\pi(1-2y+y^2)\right]\right\}\right)_y dV.\end{aligned} \tag{88}$$

The corresponding triple integral becomes

$$\begin{aligned}\alpha_6 = \frac{-\pi M_b}{2E_m^2}\int_0^l\int_0^1 &\sin\left[\frac{1}{2}\pi(1-2y+y^2)\right]\\ &\times\left(\sin^2\left[\frac{1}{2}\pi(1-2y+y^2)\right]\right.\\ &\left.\times\sin^2\left\{k_m z\,\sin\left[\frac{1}{2}\pi(1-2y+y^2)\right]\right\}\exp(2\phi)\right)_y dy dz.\end{aligned} \tag{89}$$

The partial derivative of the quantities between parentheses can be expanded into a series beginning with

$$\begin{aligned}\exp(2\phi)\big((y-1)k_m z\pi\,&\sin^2\left[\tfrac{1}{2}\pi(1-2y+y^2)\right]\cos\left[\tfrac{1}{2}\pi(1\right.\\ &\left.-2y+y^2)\right]\sin\left\{2\,\sin\left[\tfrac{1}{2}\pi(1-2y+y^2)\right]k_m z\right\}+\cdots\big),\end{aligned} \tag{90}$$

so that the integrand emerges as

$$\begin{aligned}G(z,y) = \sin\left[\tfrac{1}{2}\pi(1-2y+y^2)\right]&\exp(2\phi)\big(\pi(y-1)k_m z\\ &\times\sin^2\left[\tfrac{1}{2}\pi(1-2y+y^2)\right]\cos\left[\tfrac{1}{2}\pi(1-2y+y^2)\right]\\ &\times\sin\left\{2\,\sin\left[\tfrac{1}{2}\pi(1-2y+y^2)\right]k_m z\right\}+\cdots\big).\end{aligned} \tag{91}$$

At the outset, one can put

$$\alpha_6 = \frac{-\pi M_b}{2E_m^2}\int_0^1\int_0^l G(y,z)dz dy = \frac{-\pi M_b}{2E_m^2}\int_0^1 e^{2\phi}J(y)dy, \tag{92}$$

where a long expression is obtained for

$$J(y) = \exp(-2\phi)\int_0^l G(z,y)dz. \tag{93}$$

Using symbolic programming, one can determine the MacLaurin series expansion $J^{(0)}(y)$ for $J(y)$ (about $y=0$). To retain the proper asymptotic behavior of the viscous term, a one-term expansion $\phi\simeq-\xi y$ can be used. The closed-form solution for α_6 can then be calculated from

$$\begin{aligned}\alpha_6 &= \frac{-\pi M_b}{2E_m^2}\int_0^1 \exp(-2\xi y)J_0(y)dy\\ &= \tfrac{1}{4}\pi l M_b E_m^{-2}[1-\sin(2k_m l)/(2k_m l)]\\ &= \tfrac{1}{4}\pi l M_b E_m^{-2} = \tfrac{2}{5}M_b.\end{aligned} \tag{94}$$

Numerical estimations of α_6 confirm the weak dependence on the viscous parameter ξ. Being due to the mean flow impact on the unsteady flowfield, the inviscid character of the mean flow at leading order is clearly projected on this growth rate term.

G. Seventh factor: Viscous correction

The seventh and eighth rotational groups in Eq. (16) involve viscous damping expressions. In the classical stability calculations, viscous effects are discounted. A correction to the dilatational (volume damping) effect is represented in the seventh rotational term. This can be transformed into a surface integral, viz.,

$$\begin{aligned}&\frac{4}{3}\int\int\int_V\left\langle\delta^2\tilde{\mathbf{u}}\cdot\nabla(\nabla\cdot\hat{\mathbf{u}})\right\rangle dV\\ &\quad=-\frac{4}{3}\delta^2\int\int_S\left\langle\mathbf{n}\cdot\tilde{\mathbf{u}}\,\partial p^{(1)}/\partial t\right\rangle dS.\end{aligned} \tag{95}$$

Clearly, Eq. (95) must be negligible insofar as it scales with the product of δ^2 and the radial unsteady velocity at the boundaries.

The eighth term with viscous damping is not so negligible. Starting with

$$\alpha_7 = \frac{1}{E_m^2\exp(2\alpha_m t)}\int\int\int_V\left\langle-\delta^2(\hat{\mathbf{u}}+\tilde{\mathbf{u}})\cdot(\nabla\times\boldsymbol{\omega})\right\rangle dV, \tag{96}$$

one may set

$$\alpha_7 = \delta^2 E_m^{-2}\exp(-2\alpha_m t)\textstyle\int\int\int_V\langle A+B\rangle dV, \tag{97}$$

where $A=-\hat{\mathbf{u}}\cdot(\nabla\times\boldsymbol{\omega})$ and $B=-\tilde{\mathbf{u}}\cdot(\nabla\times\boldsymbol{\omega})$ so that

$$A = -\hat{\mathbf{u}}\cdot(\nabla\times\boldsymbol{\omega}) = e^{\alpha_m t}\sin(k_m z)\sin(k_m t)\frac{\partial^2\tilde{u}}{\partial r^2}, \tag{98}$$

$$B = -\tilde{\mathbf{u}} \cdot (\nabla \times \boldsymbol{\omega}) = e^{\alpha_m t}\left[\tilde{u}_m^r \cos(k_m t) + \tilde{u}_m^i \sin(k_m t)\right]\frac{\partial^2 \tilde{u}}{\partial r^2}. \tag{99}$$

Using standard descriptors, the second derivative can be partitioned into

$$\frac{\partial^2 \tilde{u}}{\partial r^2} = \exp(\alpha_m t)\left[\frac{\partial^2 \tilde{u}_m^r}{\partial r^2}\cos(k_m t) + \frac{\partial^2 \tilde{u}_m^i}{\partial r^2}\sin(k_m t)\right]. \tag{100}$$

Substituting back into A and B, one gathers

$$A = \sin(k_m z)\exp(2\alpha_m t)\left[\frac{\partial^2 \tilde{u}_m^r}{\partial r^2}\sin(k_m t)\cos(k_m t) + \frac{\partial^2 \tilde{u}_m^i}{\partial r^2}\sin^2(k_m t)\right] \tag{101}$$

and

$$B = \exp(2\alpha_m t)\left[\tilde{u}_m^r \frac{\partial^2 \tilde{u}_m^r}{\partial r^2}\cos^2(k_m t) + \tilde{u}_m^i \frac{\partial^2 \tilde{u}_m^i}{\partial r^2}\sin^2(k_m t) + \tilde{u}_m^r \frac{\partial^2 \tilde{u}_m^i}{\partial r^2}\cos(k_m t)\sin(k_m t) + \tilde{u}_m^i \frac{\partial^2 \tilde{u}_m^r}{\partial r^2}\cos(k_m t)\sin(k_m t)\right]. \tag{102}$$

When substituted back into Eq. (97), time averaging enables us to reduce these expressions into

$$\alpha_7 = \frac{\delta^2}{2E_m^2}\int\int\int_V \left[\tilde{u}_m^r \frac{\partial^2 \tilde{u}_m^r}{\partial r^2} + \tilde{u}_m^i \frac{\partial^2 \tilde{u}_m^i}{\partial r^2} + \sin(k_m z)\frac{\partial^2 \tilde{u}_m^i}{\partial r^2}\right] dV. \tag{103}$$

Using the same asymptotic rationale for expanding Eq. (64), one can put

$$\frac{\partial^2 \tilde{u}_m^i}{\partial r^2} \simeq \left(\frac{k_m}{M_b U_r}\right)^2 \sin(x)\exp(\phi)\cos(\psi)\sin[\sin(x)k_m z], \tag{104}$$

$$\frac{\partial^2 \tilde{u}_m^r}{\partial r^2} \simeq -\left(\frac{k_m}{M_b U_r}\right)^2 \sin(x)\exp(\phi)\sin(\psi)\sin[\sin(x)k_m z]. \tag{105}$$

The main integral becomes

$$\alpha_7 = \frac{\delta^2 k_m^2}{2E_m^2 M_b^2}\int\int\int_V \left[r^2 \csc(x)\exp(\phi)\cos(\psi)\sin(k_m z) \times \sin[k_m z \sin(x)] - r^2 \exp(2\phi)\sin^2[k_m z \sin(x)]\right] dV. \tag{106}$$

Asymptotically, it can be shown that

$$\left|r^2 \csc(x)\exp(\phi)\cos(\psi)\sin(k_m z)\sin[k_m z \sin(x)]\right| \ll \left|r^2 \exp(2\phi)\sin^2[k_m z \sin(x)]\right|. \tag{107}$$

Therefore, without any appreciable loss in accuracy, the main integral collapses into

$$\alpha_7 = \frac{-\delta^2}{2E_m^2}\left(\frac{k_m}{M_b}\right)^2 \int\int\int_V r^2 \exp(2\phi)\sin^2[k_m z \sin(x)] dV. \tag{108}$$

As usual, expanding the triple integral renders

$$\alpha_7 = \frac{-\delta^2}{2E_m^2}\left(\frac{k_m}{M_b}\right)^2 \int_0^{2\pi}\int_0^l\int_0^1 \left\{r^3 \exp(2\phi)\sin^2[k_m z \sin(x)]\right\} \times dr dz d\theta, \tag{109}$$

so that

$$\alpha_7 = \frac{-\pi\delta^2}{2E_m^2}\left(\frac{k_m}{M_b}\right)^2 \int_0^1 r^3 \exp(2\phi) \times \left[l - \frac{\sin[2k_m l \sin(x)]}{2k_m \sin(x)}\right] dr. \tag{110}$$

Recalling Eq. (12), subsequent linearization and integration lead to

$$\alpha_7 = -\tfrac{1}{8}\pi l M_b \xi^{-2} E_m^{-2}\left(1 - 2\xi + 2\xi^2 - e^{-2\xi}\right) = -\tfrac{1}{5}M_b \xi^{-2}\left(1 - 2\xi + 2\xi^2 - e^{-2\xi}\right). \tag{111}$$

At this point, it may be instructive to note that

$$1 - 2\xi + 2\xi^2 - e^{-2\xi} = \tfrac{4}{3}\xi^3 - \tfrac{2}{3}\xi^4 + \tfrac{4}{15}\xi^5 - \tfrac{4}{45}\xi^6 + O(\xi^7). \tag{112}$$

The small ξ approximation of Eq. (111) becomes

$$\alpha_7 = -\tfrac{1}{6}\pi l M_b \xi E_m^{-2}\left[1 - \tfrac{1}{2}\xi + \tfrac{1}{5}\xi^2 - \tfrac{1}{15}\xi^3 + O(\xi^4)\right] = -\tfrac{4}{15}M_b \xi\left[1 - \tfrac{1}{2}\xi + \tfrac{1}{5}\xi^2 - \tfrac{1}{15}\xi^3 + O(\xi^4)\right]. \tag{113}$$

In turbulent flow, one can expect the impact of α_6 and α_7 on stability to become markedly more significant.

H. Eighth factor: Pseudoacoustical correction

The last two terms in Eq. (16) are due to the coupling between the pseudopressure associated with the vortical field and either the unsteady acoustical or rotational velocities. The first term can be expressed by

$$\alpha_8 = \frac{1}{E_m^2 \exp(2\alpha_m t)}\int\int\int_V \langle -\hat{\mathbf{u}} \cdot \nabla \tilde{p}\rangle dV. \tag{114}$$

Traditionally, terms due to the pseudopressure are ignored because of the small contribution of $\tilde{p}$.[33,36] At present, the corresponding integrals will be evaluated before a decision is made. Our motivation stems from recent numerical and experimental studies that have emphasized the importance of the pseudopressure in the global analysis.[37–40]

Following the form used in Eq. (20), one can write

$$\tilde{p} = \exp(\alpha_m t)\left[\tilde{p}_m^r \cos(k_m t) + \tilde{p}_m^i \sin(k_m t)\right], \tag{115}$$

where

$$\tilde{p}_m^r = -\tfrac{1}{2}\pi M_b z \sin(\psi)\sin(2x)\exp(\phi)\sin[k_m z \sin(x)], \tag{116}$$

$$\tilde{p}_m^i = \tfrac{1}{2}\pi M_b z \cos(\psi)\sin(2x)\exp(\phi)\sin[k_m z \sin(x)]. \tag{117}$$

Accordingly,

$$\nabla\tilde{p} = \exp(\alpha_m t)\left[\cos(k_m t)\,\nabla\,\tilde{p}_m^r + \sin(k_m t)\,\nabla\,\tilde{p}_m^i\right], \tag{118}$$

$$\begin{aligned}\nabla\tilde{p}_m^r &= \frac{\partial}{\partial r}(\tilde{p}_m^r)\mathbf{e}_r + \frac{\partial}{\partial z}(\tilde{p}_m^r)\mathbf{e}_z \\ &\simeq -\tfrac{1}{2}\pi(k_m/U_r)z\cos(\psi)\sin(2x)\exp(\phi)\sin[k_m z\sin(x)] \\ &\quad\times\mathbf{e}_r - \tfrac{1}{2}\pi M_b \sin(\psi)\sin(2x)\exp(\phi)\{\sin[k_m z\sin(x)] \\ &\quad + k_m z\sin(x)\cos[k_m z\sin(x)]\}\mathbf{e}_z\end{aligned} \tag{119}$$

and

$$\begin{aligned}\nabla\tilde{p}_m^i &= \frac{\partial}{\partial r}(\tilde{p}_m^i)\mathbf{e}_r + \frac{\partial}{\partial z}(\tilde{p}_m^i)\mathbf{e}_z \\ &\simeq -\tfrac{1}{2}\pi(k_m/U_r)z\sin(\psi)\sin(2x)\exp(\phi)\sin[k_m z\sin(x)] \\ &\quad\times\mathbf{e}_r + \tfrac{1}{2}\pi M_b \cos(\psi)\sin(2x)\exp(\phi)\{\sin[k_m z\sin(x)] \\ &\quad + k_m z\sin(x)\cos[k_m z\sin(x)]\}\mathbf{e}_z.\end{aligned} \tag{120}$$

Before time averaging, the integrand in α_8 can be expanded into

$$\begin{aligned}\hat{\mathbf{u}}\cdot\nabla\tilde{p} &\simeq \tfrac{1}{2}\pi M_b \exp(2\alpha_m t)\sin(k_m z)\sin(k_m t)\sin(2x) \\ &\quad\times\exp(\phi)\{\sin[k_m z\sin(x)] \\ &\quad + k_m z\sin(x)\cos[k_m z\sin(x)]\} \\ &\quad\times[\cos(\psi)\sin(k_m t) - \sin(\psi)\cos(k_m t)].\end{aligned} \tag{121}$$

Hence,

$$\begin{aligned}\langle\hat{\mathbf{u}}\cdot\nabla\tilde{p}\rangle &= \tfrac{1}{4}\pi M_b \exp(2\alpha_m t)\sin(k_m z)\sin(2x)e^{\phi}\cos(\psi) \\ &\quad\times\{\sin[k_m z\sin(x)] \\ &\quad + k_m z\sin(x)\cos[k_m z\sin(x)]\}.\end{aligned} \tag{122}$$

The corresponding integral becomes

$$\begin{aligned}\alpha_8 &= -E_m^{-2}\iiint_V \tfrac{1}{4}\pi M_b \exp(\phi)\sin(k_m z)\sin(2x)\cos(\psi) \\ &\quad\times\{\sin[k_m z\sin(x)] + k_m z\sin(x)\cos[k_m z\sin(x)]\}dV,\end{aligned} \tag{123}$$

which can be evaluated from

$$\begin{aligned}\alpha_8 &= -\frac{1}{4}\pi M_b E_m^{-2}\int_0^{2\pi}\int_0^l\int_0^1 r\sin(k_m z)\sin(2x)e^{\phi}\cos(\psi) \\ &\quad\times\{\sin[k_m z\sin(x)] + k_m z\sin(x) \\ &\quad\times\cos[k_m z\sin(x)]\}drdzd\theta \\ &= -\frac{1}{2}\pi^2 M_b E_m^{-2} \\ &\quad\times\int_0^l\int_0^1 r\sin(k_m z)\sin(2x)\exp(\phi)\cos(\psi) \\ &\quad\times\{\times\sin[k_m z\sin(x)] \\ &\quad + k_m z\sin(x)\cos[k_m z\sin(x)]\}drdz.\end{aligned} \tag{124}$$

At this juncture, one can directly integrate Eq. (124) with respect to z. The outcome is

$$\alpha_8 = -\frac{1}{4}\pi^2 M_b k_m^{-1} E_m^{-2}\int_0^1 Q(r)dr, \tag{125}$$

where

$$\begin{aligned}Q(r) &= r\exp(\phi)\cos(\psi)\sin(2x)\sec^3(x)\big(\cos(k_m l) \\ &\quad\times\{-2k_m l\cos(x)\cos[k_m l\sin(x)]\sin(x) \\ &\quad + [\cos(2x)-3]\sin^2(x)\sin[k_m l\sin(x)] \\ &\quad - 2\cos[k_m l\sin(x)]\tan(x)\}\big).\end{aligned} \tag{126}$$

The result must then be linearized and integrated with respect to r. One obtains

$$\begin{aligned}\alpha_8 &\simeq -\frac{1}{24}\pi^3 l M_b E_m^{-2}\int_0^1 \exp(-\xi y)\cos(k_m y/M_b) \\ &\quad\times\left\{\left[2(\pi k_m l)^2 - \pi^2 + 3\right]y^3 - 9y^2 + 6y\right\}dy,\end{aligned} \tag{127}$$

and so

$$\begin{aligned}\alpha_8 &= \tfrac{1}{4}\pi^3 l M_b^3 k_m^{-2} E_m^{-2}(1 + M_b^2\xi^2/k_m^2)^{-3}\left\{1 - M_b^2 k_m^{-2}\left[9\xi\right.\right. \\ &\quad\left.\left. + (3 - \pi^2 + 2\pi^2 k_m^2 l^2)(1 + M_b^2\xi^2/k_m^2)^{-1}\right]\right\} + O(M_b^7 k_m^{-6}).\end{aligned} \tag{128}$$

Using $k_m = m\pi/l$ and Eq. (27), α_8 can be rearranged into

$$\begin{aligned}\alpha_8 &= \tfrac{2}{5}(M_b^3 l^2/m^2)\left[1 + M_b^2\xi^2 l^2/(m\pi)^2\right]^{-3}\left\{1 - M_b^2 l^2/(m\pi)^2\right\} \\ &\quad\times\left\{9\xi + (3 - \pi^2 + 2\pi^4 m^2)\left[1 + M_b^2\xi^2 l^2/(m\pi)^2\right]^{-1}\right\}.\end{aligned} \tag{129}$$

In most rocket motor applications exhibiting a relatively small ξ, α_8 may be given by

$$\alpha_8 = \tfrac{2}{5}(M_b^3 l^2/m^2)[1 - 3M_b^2\xi^2 l^2/(m\pi)^2]. \tag{130}$$

It may be interesting to note that the leading-order inviscid part, namely, $\alpha_8^0 = \frac{2}{5}(M_b^3 l^2/m^2)$ is always smaller than $\alpha_1, \alpha_4, \alpha_5, \alpha_6$, or α_7. Nonetheless, since α_8 remains larger in magnitude than $\alpha_2 = -\frac{8}{15}\xi M_b^3$, its inclusion in the overall stability assessment is helpful for methodological consistency.

I. Ninth factor: Pseudorotational correction

As alluded to earlier, the last term in Eq. (16) is due to the less obvious coupling that is formed between vorticity-induced pseudopressure and the unsteady rotational velocity. The significance of this term can be derived from

$$\alpha_9 = \frac{-1}{E_m^2\exp(2\alpha_m t)}\int\int\int_V \langle\tilde{\mathbf{u}}\cdot\nabla\tilde{p}\rangle dV. \tag{131}$$

After taking the dot product of Eqs. (20) and (118), one carries out the time averaging to obtain

$$\langle \tilde{\mathbf{u}} \cdot \nabla \tilde{p} \rangle = -\tfrac{1}{4}\pi M_b \exp(2\alpha_m t)\big(\sin(2x)\sin(x)\exp(2\phi) \times\{\sin[k_m z \sin(x)] + k_m z \sin(x) \times\cos[k_m z \sin(x)]\}\sin[k_m z \sin(x)] + k_m z \sin^2(x)\sin(2x)\exp(2\phi)\sin[k_m z \sin(x)] \times\cos[k_m z \sin(x)]\big). \quad (132)$$

The volume integral becomes

$$\alpha_9 = \tfrac{1}{4}\pi M_b E_m^{-2}\iiint_V \big(\sin(2x)\sin(x)\exp(2\phi) \times\{\sin[k_m z \sin(x)] + k_m z \sin(x)\cos[k_m z \sin(x)]\} \times\sin[k_m z \sin(x)] + k_m z \sin^2(x)\sin(2x) \times\exp(2\phi)\sin[k_m z \sin(x)]\cos[k_m z \sin(x)]\big) dV, \quad (133)$$

and so,

$$\alpha_9 = \frac{1}{2}\pi^2 M_b E_m^{-2}\int_0^1\int_0^1 r\big(\sin(2x)\sin(x)\exp(2\phi) \times\{\sin[k_m z \sin(x)] + k_m z \sin(x)\cos[k_m z \sin(x)]\} \times\sin[k_m z \sin(x)] + k_m z \sin^2(x)\sin(2x) \times\exp(2\phi)\sin[k_m z \sin(x)]\cos[k_m z \sin(x)]\big) dr dz. \quad (134)$$

Next, the integral with respect to z is evaluated. The subsequent expression is transformed into y, linearized near the wall, and integrated term-by-term. After some effort, one finds

$$\alpha_9 = \frac{1}{4}\pi^2 l M_b E_m^{-2}\int_0^1 \Bigg[(1-y)\exp(2\phi) \times\left(1-\cos\left\{2k_m l \sin\left[\frac{1}{2}\pi(1-2y+y^2)\right]\right\}\right) \times\sin\left[\frac{1}{2}\pi(1-2y+y^2)\right]\sin\big[\pi(1-2y+y^2)\big]\Bigg] dy. \quad (135)$$

Equation (135) requires an asymptotic treatment that relies, in part, on trigonometric identities. One collects

$$\alpha_9 = \frac{9}{50}\pi l M_b E_m^{-2}\int_0^1 \exp(2\phi)(1-y) \times\left\{\cos\left[\frac{1}{2}\pi(1-2y+y^2)\right] - \cos\left[\frac{3}{2}\pi(1-2y+y^2)\right]\right\} dy, \quad (136)$$

thus leaving us with

$$\alpha_9 = \frac{9}{50}\pi l M_b E_m^{-2}\int_0^1 \exp(-2\xi y)(2\pi y - \pi y^2)(1-y) dy, \quad (137)$$

which, at length, gives

$$\alpha_9 = \tfrac{9}{200}\pi^2 l M_b E_m^{-2}\big[\big(\xi^2 - \tfrac{3}{2}\big)\exp(-2\xi) + \tfrac{3}{2} - 3\xi + 2\xi^2\big]\xi^{-4} = \tfrac{9}{125}\pi M_b\big[\big(\xi^2 - \tfrac{3}{2}\big)\exp(-2\xi) + \tfrac{3}{2} - 3\xi + 2\xi^2\big]\xi^{-4}. \quad (138)$$

In seeking the small ξ approximation, it is helpful to note that

$$\big(\xi^2 - \tfrac{3}{2}\big)e^{-2\xi} + \tfrac{3}{2} - 3\xi + 2\xi^2 = \xi^4 - \tfrac{14}{15}\xi^5 + \tfrac{8}{15}\xi^6 + \cdots. \quad (139)$$

At the outset, Eq. (138) can be expanded into

$$\alpha_9 = \tfrac{9}{125}\pi M_b\big(1 - \tfrac{14}{15}\xi + \tfrac{8}{15}\xi^2 - \tfrac{8}{35}\xi^3 + \tfrac{5}{63}\xi^4 + \cdots\big), \quad (140)$$

whose leading order can be seen to be $\alpha_9^0 = \frac{9}{125}\pi M_b$. Being of the same order as $\alpha_1, \alpha_4, \alpha_5, \alpha_6$, or α_7, the pseudorotational correction constitutes an important destabilizing factor that requires incorporation into the stability calculations. The appearance of such a term lends further support to the recent experimental and numerical findings of French investigators.[37–40] The present study confirms that, despite the small size of the pseudopressure by comparison with the acoustic component, its incorporation throughout the analysis is necessary for the accurate appropriation of coupling with essential flow elements. When gauging α_8 and α_9, the latter is more appreciable. The most significant contribution is owed, once again, to the presence of an unsteady rotational field. This justifies, in part, the omission of the pseudopressure in stability calculations based on an oscillatory field that lacks the boundary-driven rotational element. So far this principal flow ingredient has given rise to six growth rate corrections via α_4 through α_9.

J. Tenth factor: Unsteady nozzle correction

One term that has often been omitted in stability calculations is due to the unsteady rotational energy exiting the motor at the downstream end. This growth rate is precipitated by the third and fourth rotational terms of Eq. (16); these can be lumped together via

$$\alpha_{10} = \frac{-M_b}{E_m^2 \exp(2\alpha_m t)}\int\int\int_V \langle(\hat{\mathbf{u}} + \tilde{\mathbf{u}}) \cdot \nabla(\mathbf{U}\cdot\tilde{\mathbf{u}})\rangle dV. \quad (141)$$

This triple integral can be converted into

$$\alpha_{10} = -M_b E_m^{-2} e^{-2\alpha_m t}\int\int_{S_N}\big\langle\big[\mathbf{n}\cdot(\hat{\mathbf{u}} + \tilde{\mathbf{u}})\big](\mathbf{U}\cdot\tilde{\mathbf{u}})\big\rangle dS = -M_b E_m^{-2} e^{-2\alpha_m t}\int\int_{S_N}\big\langle\tilde{u}_z^2 U_z\big\rangle dS + O(M_b^2) = -M_b E_m^{-2} e^{-2\alpha_m t}\int\int_{S_N}\big\langle e^{2\alpha_m t}\pi z\cos(x)\big[(\tilde{u}_m^r)^2 \times\cos^2(k_m t) + (\tilde{u}_m^i)^2\sin^2(k_m t) + 2\tilde{u}_m^r\tilde{u}_m^t\sin(k_m t) \times\cos(k_m t)\big]\big\rangle dS, \quad (142)$$

which, after time averaging, renders

TABLE I. Linear growth rate corrections and the critical parameters delineating stability boundaries.

	Improved rotational set in general form	Evaluated growth rates (dimensionless)
	$E_m^2=\frac{1}{2}\int\int\int[(\hat{p}_m)^2+\hat{\boldsymbol{u}}_m\cdot\hat{\boldsymbol{u}}_m+2\hat{\boldsymbol{u}}_m\cdot\boldsymbol{u}_m^i+\boldsymbol{u}_m^r\cdot\boldsymbol{u}_m^r+\boldsymbol{u}_m^i\cdot\boldsymbol{u}_m^i]dV$	
α_1: Pressure coupling	$-E_m^{-2}\exp(-2\alpha_m t)\int\int\int_V\langle\nabla\cdot[\hat{p}\hat{\boldsymbol{u}}+\frac{1}{2}M_b\boldsymbol{U}(\hat{p})^2]+M_b[\hat{\boldsymbol{u}}\cdot\nabla(U\cdot\hat{\boldsymbol{u}})]\rangle dV$	$\frac{4}{5}M_b[A_b^{(r)}-\gamma]$
α_2: Dilatational	$E_m^{-2}\exp(-2\alpha_m t)\int\int\int_V\langle\frac{4}{3}\delta^2\hat{\boldsymbol{u}}\cdot\nabla(\nabla\cdot\hat{\boldsymbol{u}})\rangle dV$	$-\frac{8}{15}\xi M_b^3\ll O(1)$
α_3: Acoustic mean	$E_m^{-2}\exp(-2\alpha_m t)\int\int\int_V\langle M_b\{\hat{\boldsymbol{u}}\cdot(\hat{\boldsymbol{u}}\times\Omega)\}\rangle dV$	0
α_4: Flow turning	$E_m^{-2}\exp(-2\alpha_m t)\int\int\int_V\langle M_b\hat{\boldsymbol{u}}\cdot(\boldsymbol{U}\times\omega)\rangle dV$	$-\frac{4}{5}M_b(1+\pi^{-2}M_b^2\xi^2l^2m^{-2})^{-1}$
α_5: Rotational flow	$-E_m^{-2}\exp(-2\alpha_m t)\int\int\int_V\langle\boldsymbol{u}\cdot\nabla\hat{p}\rangle dV$	$\frac{4}{5}M_b(1+\pi^{-2}M_b^2\xi^2l^2m^{-2})^{-1}$
α_6: Mean vorticity	$E_m^{-2}\exp(-2\alpha_m t)\int\int\int_V\langle M_b\boldsymbol{u}\cdot(\boldsymbol{U}\times\omega)\rangle dV$	$\frac{2}{5}M_b$
α_7: Viscosity	$-E_m^{-2}\exp(-2\alpha_m t)\int\int\int_V\langle\delta^2(\hat{\boldsymbol{u}}\cdot\boldsymbol{u})\cdot(\nabla\times\omega)\rangle dV$	$-\frac{4}{15}M_b\xi[1-\frac{1}{2}\xi+\frac{1}{5}\xi^2-\frac{1}{15}\xi^3+O(\xi^4)]$
α_8: Pseudo acoustic	$E_m^{-2}\exp(-2\alpha_m t)\int\int\int_V\langle-\hat{\boldsymbol{u}}\cdot\nabla p\rangle dV$	$\frac{2}{5}(M_b^3l^2/m^2)\ll O(1)$
α_9: Pseudo vorticity	$-E_m^{-2}\exp(-2\alpha_m t)\int\int\int_V\langle\boldsymbol{u}\cdot\nabla p\rangle dV$	$\frac{9}{125}\pi M_b[(\xi^2-\frac{3}{2})\exp(-2\xi)+\frac{3}{2}-3\xi+2\xi^2]\xi^{-4}$
α_{10}: Unsteady nozzle	$-E_m^{-2}\exp(-2\alpha_m t)\int\int\int_V\langle M_b(\hat{\boldsymbol{u}}+\boldsymbol{u})\cdot\nabla(\boldsymbol{U}\cdot\boldsymbol{u})\rangle dV$	$-\frac{4}{3}\pi M_b\{[\pi^2+4(\xi+\sqrt{2})^2]^{-1}-\frac{1}{500}\}$
Critical damping parameter	$\xi_r=-3\gamma_b+\sqrt{9\gamma_b^2+12M_b^2}/(4M_b^2)$	
Critical aspect ratio	$l_r=m\pi\delta M_b^{-3/2}/\sqrt{\frac{5}{6}+\frac{\sqrt{35}}{3}\sinh(\frac{1}{3}\sinh^{-1}\{4[\frac{325}{4}+27(-\frac{15}{2}-15\gamma_b)]/(35\sqrt{35})\})}$	
Critical Mach number	$M_{br}=\sqrt{6\{\frac{1}{2}-\gamma_b-[\frac{1}{4}\xi^{-2}(1-2\xi+2\xi^2-e^{-2\xi})]\}}\sqrt{(4\xi-3l^2/m^2)}$	

$$\alpha_{10}=-\frac{1}{2}\pi M_b E_m^{-2}\int\int_{S_N} z\cos x\left[(\tilde{u}_m^r)^2+(\tilde{u}_m^l)^2\right]dS$$
$$=-\pi^2 l M_b E_m^{-2}\int_0^1 e^{2\phi}r\cos x\sin^2 x\sin^2(k_m l\sin x)dr. \tag{143}$$

Subsequent integration yields

$$\alpha_{10}=-\pi^2 l M_b E_m^{-2}\int_0^1(1-y)\exp(-2\xi y)\times\cos\left[\tfrac{1}{2}\pi(1-2y+y^2)\right]\times\sin^2\left[\tfrac{1}{2}\pi(1-2y+y^2)\right]\times\sin^2\left\{k_m l\sin\left[\tfrac{1}{2}\pi(1-2y+y^2)\right]\right\}dy. \tag{144}$$

At this point, one may prove that α_{10} is identical to $-\alpha_9$ (for a full length motor) by using the trigonometric identities

$$\sin^2\left\{k_m l\sin\left[\tfrac{1}{2}\pi(1-2y+y^2)\right]\right\}=\tfrac{1}{2}\left(1-\cos\left\{2k_m l\sin\left[\tfrac{1}{2}\pi(1-2y+y^2)\right]\right\}\right),$$
$$\cos\left[\tfrac{1}{2}\pi(1-2y+y^2)\right]\sin\left[\tfrac{1}{2}\pi(1-2y+y^2)\right]=\tfrac{1}{2}\sin\left[\pi(1-2y+y^2)\right]. \tag{145}$$

These will transform Eq. (144) into the negative of Eq. (135). The last squared sine term in Eq. (144) causes α_{10} (and, in retrospect, α_9) to be virtually independent of $k_m l$. Supported by numerical verification, one finds α_{10} to be a sole function of ξ. Based on Eq. (144) an alternative approximation that is more accurate for $\xi\leqslant 7$ can be found by using the Lorentzian form

$$\alpha_{10}=-\frac{5}{6}\pi^2 l M_b E_m^{-2}\left\{\left[\pi^2+4\left(\xi+\sqrt{2}\right)^2\right]^{-1}-\frac{1}{500}\right\}$$
$$=-\frac{4}{3}\pi M_b\left\{\left[\pi^2+4\left(\xi+\sqrt{2}\right)^2\right]^{-1}-\frac{1}{500}\right\}. \tag{146}$$

One may check that the inviscid limit is $\alpha_{10}^0=-\frac{9}{125}\pi M_b$, hence equal but opposite in sign to α_9^0. Despite their widely dissimilar sources, it is interesting that both α_9 and α_{10} cancel identically when the summation is performed over a full length cylindrical motor. This result remains approximate because compressibility effects in the nozzle section are not accounted for. Specifically, we have adopted the classic notion of a nozzleless, incompressible mean flow, an assumption that degenerates near the nozzle entrance. It is hoped that a judicious model for nozzle performance can be later developed and appended to the current formulation. Work in that direction is currently underway.

IV. DISCUSSION

A. Irrotational stability formulation

The collection of irrotational and rotational growth rate factors is summarized in Table I. To assess the degree of improvement associated with the current results, one may compare the predictions of irrotational stability formulations with those proposed here. For illustrative purposes, one may choose four representative cases that have been regularly cited in the literature.[13] These cases span a practical range of

TABLE II. Physical parameters for representative motors.

Motor	L(m)	R(m)	M_b	δ	k_m	S	ξ	f(Hz)	$A_b^{(r)}$	a_0(m/s)
Small motor	0.60	0.025	1.7^{-3}	5.49^{-4}	1.31^{-1}	77.00	1.0512	1227	2.5	1472
Tactical rocket	2.03	0.102	3.1^{-3}	2.74^{-4}	1.58^{-1}	50.92	0.0628	360	1.2	1462
Cold flow	1.73	0.051	3.3^{-3}	6.07^{-4}	9.26^{-2}	28.07	0.0879	84.0	−2.0[a]	291
Space shuttle SRB	35.1	0.700	2.3^{-3}	1.04^{-4}	6.27^{-2}	27.24	0.0035	19.5	1.0	1369

[a]Assumed value due to the absence of a reported estimate.

operating parameters for select rocket motors and cold-flow experiments. In the interest of clarity, these parameters are cataloged in Table II. As indicated earlier, some stability algorithms do not retain unsteady rotational effects except through the flow turning loss. The growth rate predicted by such models is based on

$$\alpha_i = \alpha_{1-4} = -\tfrac{1}{2}\pi l \gamma_b M_b E_m^{-2} - \tfrac{1}{3}\pi k_m^2 l \delta^2 E_m^{-2} - \tfrac{1}{2}\pi l M_b E_m^{-2}\left(1 + M_b^2 \xi^2 / k_m^2\right)^{-1}, \tag{147}$$

where the subscript i refers to the irrotational formulation, and $\gamma_b \equiv \gamma - A_b^{(r)}$. Recalling that the irrotational energy normalization is given by $(E_m^2)_i = \frac{1}{2}\pi L/R$, Eq. (147) can be put in the form $\alpha_{1-4} = K_i M_b$; the irrotational growth rate coefficient is simply

$$K_i = -\gamma_b - \tfrac{2}{3}\xi M_b^2 - \left[1 + M_b^2 \xi^2 l^2/(m^2\pi^2)\right]^{-1}. \tag{148}$$

Clearly, the sign of K_i will directly prescribe motor stability (according to the standard formulation). Interestingly, it is possible for the sign of K_i to remain constant as ξ is increased over the interval $10^{-3}-10^3$. It is also possible for K_i to change sign, specifically, from negative to positive, as ξ is increased. The key lies in Cardano's discriminant for $K_i = 0$, namely,

$$\Delta_i = 9l^2(1+\gamma_b)\gamma_b^3 + m^2\pi^2[27 + 4\gamma_b(9+2\gamma_b)]M_b^2. \tag{149}$$

When $\Delta_i < 0, K_i$ will change sign at the critical damping parameter of

$$\xi_i = \Big[\sqrt{\gamma_b^2 - \tfrac{4}{3}m^2\pi^2 M_b^2 l^{-2}} \times \sin\Big(\tfrac{1}{3}\sin^{-1}\Big\{\Big(\gamma_b^2 - \tfrac{4}{3}m^2\pi^2 M_b^2 l^{-2}\Big)^{-3/2} \times \Big[\gamma_b^3 + (6+4\gamma_b)m^2\pi^2 M_b^2 l^{-2}\Big]\Big\}\Big) - \tfrac{1}{2}\gamma_b\Big] M_b^{-2}. \tag{150}$$

It may be instructive to note that whenever $\gamma_b < -1 (\Delta_i > 0), K_i$ will be negative, hence indicating a stable system. However, when $\Delta_i < 0$, an unstable system is realized for $\xi > \xi_i$; it appears that the standard formulation is missing an important element so long as friction has a damping rather than an energizing effect. Physically, increasing ξ at a given oscillation mode number should have a stabilizing impact because it can only be accomplished by increasing the dimensionless viscosity δ, decreasing the surface Mach number, or decreasing the length of the motor.

For small ξ, K_i may be expanded into

$$K_i = -\gamma_b - 1 + \xi M_b^2\left[\xi l^2/(m^2\pi^2) - \tfrac{2}{3}\right] + O(M_b^4 \xi^4 l^4). \tag{151}$$

It follows that, for motors exhibiting small ξ, α_{1-4} is expressible by

$$\alpha_{1-4}^0 \simeq -M_b(\gamma_b + 1) + \xi M_b^3\left[\xi l^2/(m^2\pi^2) - \tfrac{2}{3}\right]. \tag{152}$$

B. Rotational formulation

For a more precise stability estimation, one may use the subscript r for "rotational" and write

$$\alpha_r = \alpha_{1-10} = \sum_{n=1}^{10} \alpha_n, \tag{153}$$

where the energy normalization is based on[33]

$$(E_m^2)_r = \tfrac{5}{8}\pi L/R. \tag{154}$$

The superposition of these terms yields $\alpha_{1-10} = \frac{4}{5}M_b K_r$; the rotational stability coefficient is realizable from

$$K_r = -\gamma_b + \tfrac{1}{2} - \xi\left[\tfrac{2}{3}M_b^2 + \tfrac{1}{4}\xi^{-3}\left(1 - 2\xi + 2\xi^2 - e^{-2\xi}\right)\right] + \tfrac{1}{2}(M_b^2 l^2/m^2)\left[1 + M_b^2\xi^2 l^2/(m\pi)^2\right]^{-3}. \tag{155}$$

Equation (155) enables us to seek direct relations between chamber parameters that will ensure a stable system by guaranteeing a negative K_r. Similar relations can be helpful in the developmental stages of motors exhibiting less simplistic grain configurations. Using a cubic expansion of K_r near $\xi = 0$, one collects, at $O(\xi^4, M_b^6)$,

$$K_r^0 = -\gamma_b + \tfrac{1}{2} - \tfrac{1}{3}\xi + \tfrac{1}{6}\xi^2 - \tfrac{1}{15}\xi^3 + \tfrac{1}{2}M_b^2\left[l^2/m^2 - \tfrac{4}{3}\xi - 3M_b^2\xi^2 l^4/(m^4\pi^2)\right]. \tag{156}$$

This expression is valid for $\xi \leqslant 1, M_b \leqslant 0.1$. However, dismissing the last term in Eq. (156) merely reduces its range to $M_b \leqslant 0.01$. This simpler relation is useful in predicting the onset of instability in motors with small ξ. Insofar as the critical value ξ_r that causes K_r^0 to change sign is the zero of Eq. (156), one can use Cardano's method to find the useful expression

$$\xi_r = \tfrac{5}{6} + \tfrac{\sqrt{35}}{3}\sinh\Big[\tfrac{1}{3}\sinh^{-1}\Big(4\Big\{\tfrac{325}{4} + 27\Big[-\tfrac{15}{2} - 15\gamma_b - 15M_b^2 l^2/(2m^2)\Big]\Big\}/(35\sqrt{35})\Big)\Big], \quad \xi_r \leqslant 1.0. \tag{157}$$

To promote a stable system, one must have $\xi > \xi_r$ for a given set of parameters. Thus, for sufficiently small ξ and M_b, the growth rate collapses, at $O(\xi^2, M_b^2)$, into

$$\alpha_{1-10}^0 = \tfrac{4}{5}M_b\left(-\gamma_b + \tfrac{1}{2} - \tfrac{1}{3}\xi\right). \tag{158}$$

In a similar way, one can seek a quadratic expansion of K_r for large ξ. This yields an approximation that is valid for $\xi > 10, M_b \leqslant 0.1$. The corresponding K_r^∞ at $O(\xi^{-3})$ becomes

TABLE III. Numerical integrals of irrotational, rotational, and individual growth rates (s^{-1}).

Motor	α^*_{1-4} [a]	α^*_{1-10}	$\lvert\Delta\alpha\rvert$ (s^{-1})	α^*_1	α^*_2	α^*_4	α^*_5	α^*_6	α^*_7	α^*_8	α^*_9	α^*_{10}
Small motor	20.1	116	82.7	96.1	-1.62^{-4}	−80.0	80.0	39.2	−19.00	0.0650	11.5	−11.5
Tactical rocket	−49.1	12.4	79	−3.55	-1.43^{-5}	−35.7	35.7	16.5	−0.716	0.0630	9.62	−9.62
Cold flow	−81.3	−43.0	38.3	−49.7	-9.63^{-6}	−15.3	15.3	7.02	−0.419	0.0490	4.01	−4.01
Space shuttle SRB	−5.93	.600	6.53	−1.08	-4.43^{-8}	−3.66	3.66	1.66	−0.004 11	0.0113	1.01	−1.01

[a]The sum of the growth rates is multiplied by 5/4 to be consistent with the irrotational stability formulation based on an energy normalization value of $(E^2_m)_i=\frac{1}{2}\pi L/R$ instead of $(E^2_m)_r=\frac{5}{8}\pi L/R$.

$$K^{\infty}_r = -\gamma_b + \tfrac{1}{2}\xi^{-1} - \tfrac{2}{3}M^2_b\xi. \tag{159}$$

In calculating the critical value ξ_r that causes K^{∞}_r to vanish, root finding methods can also be used to obtain

$$\xi_r = -3\gamma_b + \sqrt{9\gamma^2_b + 12M^2_b}/(4M^2_b), \quad \xi_r > 10. \tag{160}$$

Along similar lines, the critical Mach number which must not be exceeded lest instabilities occur can be calculated using a quadratic approximation to $O(M^2_b l^2 \xi^2)$; we get

$$M_{br} = \sqrt{6C_r(4\xi - 3l^2/m^2)},$$
$$C_r = \tfrac{1}{2} - \gamma_b - \left[\tfrac{1}{4}\xi^{-2}(1 - 2\xi + 2\xi^2 - e^{-2\xi})\right]. \tag{161}$$

If needed, a higher-order approximation that does not ignore any terms in Eq. (155) can also be obtained,

$$M_{br} = \frac{D_r}{18C_r l^6 \xi^6 2^{1/3}} - \frac{m^2\pi^2}{l^2\xi^2} - \frac{2^{1/3}(3l^2-2)}{D_r}, \tag{162}$$

where

$$D_r = [2916C_r l^{12} m^2 \pi^2 \xi^{10} + 1944C^2_r l^{10} m^2 \pi^2 \xi^{11} + \sqrt{4c^3_r(54l^8\xi^6 + 36l^6\xi^7)^3 + C^4_r m^4 \pi^4 (2916l^{12}\xi^{10} + 1944l^{10}\xi^{11})^2}]^{1/3}. \tag{163}$$

C. Comparing numerics and asymptotics

Results are illustrated in Tables III and IV using dimensional growth rates. These are related to the nondimensional values via $\alpha^* = \alpha a_0/R$. In Table III, all factors are computed by numerically evaluating the volume integrals. In Table IV, the analytical expressions derived earlier are used to estimate the corresponding factors. From these tables, one realizes that a non-negligible difference exists between the α^*_{1-4} and the rotationally adjusted value α^*_{1-10}. More importantly, the discrepancy suggests, in every instance, a less stable system than projected by an irrotational model. The additional rotational corrections are seemingly essential to the proper assessment of instability, particularly, in the early stages of motor development.

The suitability of analytical approximations in reproducing the numerically integrated growth rate factors can be extrapolated from Table IV. By comparison with numerics, asymptotic expressions derived here exhibit small errors of 1.72%, 8.87%, and 1.16% for the small motor, tactical rocket, and cold-flow cases, respectively. These trends are typical of rocket motor configurations and cold-flow simulations. However, for the shuttle solid rocket booster (SRB), a maximum error of 23.3% is realized, mainly due to the smallness of α^*_{1-10}. This relative error is somewhat misleading in view of the fact that the SRB case exhibits the smallest absolute error of the four representative growth rate factors. Clearly, the relative truncation error in the shuttle SRB case is inflated due to the smaller than usual value of α^*_{1-10}. In

TABLE IV. Analytical estimates of irrotational, rotational, and individual growth rates (s^{-1}).

Motor	α^*_{1-4} [a]	α^*_{1-10}	$\lvert\Delta\alpha\rvert$ (s^{-1})	α^*_1	α^*_2	α^*_4	α^*_5	α^*_6	α^*_7	α^*_8	α^*_9	α^*_{10}
Small motor	20.0	118	98.2	96.1	-1.62^{-4}	−80.1	80.1	40.0	−17.90	0.0644	11.4	−11.4
Tactical rocket	−48.9	13.5	62.4	−3.55	-1.43^{-5}	−35.5	35.5	17.8	−0.721	0.0627	9.64	−9.64
Cold flow	−81.0	−42.5	38.5	−49.7	-9.63^{-6}	−15.1	15.1	7.53	−0.423	0.0717	4.02	−4.02
Space shuttle SRB	−5.85	.740	6.59	−1.08	-4.43^{-8}	−3.60	3.60	1.80	−0.004 18	0.0179	1.01	−1.01

[a]Same as in Table II.

fact, the maximum absolute error rather occurs in the small motor case with the largest value of ξ. It should also be noted that the agreement between numerics and asymptotics improves in α_7^*, and does not change in α_6^* as $\xi\to\infty$. The accuracy of the analytical approximation also improves in α_7^* but deteriorates in α_8^* as L/R is increased. The discrepancy in α_8^* at large L/R does not pose a problem due to the small contribution of α_8^*.

D. Growth rate sensitivity

The availability of both numerical and analytical representations of the composite rotational growth rate enables us to examine its sensitivity to different ranges of the operating parameters. Specifically, one may study its sensitivity to variations in $(M_b, L/R, m)$ and ξ (or δ) at constant γ_b. Later, the influence of γ_b will be separately examined. To start, one may want to vary the oscillation mode number for fixed values of $L/R, \xi$, and the Mach number. Recalling that $k_m = m\pi R/L$, increasing m is equivalent to increasing the wave number k_m. For every value of L/R, the first two oscillation modes lead to two increasing values of k_m. Similarly, since $\xi = m^2\pi^2\delta^2 M_b^{-3} R^2/L^2$, the viscous parameter can be decreased at constant δ by increasing the chamber aspect ratio. As L/R is varied from 1 to 100, the influence of viscous damping can be captured by plotting the results at two different Mach numbers. This is accomplished in Fig. 4 where the numerically integrated values of α_{1-10} are displayed at four distinct values of δ. In these computations, $\gamma_b = -0.45$ is fixed because a value of $\gamma = 1.3$ is used along with a dimensionless surface admittance of $A_b^{(r)} = 1.75$; the latter represents the average of reported values (for live propellants) ranging from 1.0 to 2.5 in Table II.

Figure 4 indicates that increasing δ increases the system stability by leading to an increasingly more negative α_{1-10}. As mass injection is increased, the curves for $\delta = 10^{-4}$ and 10^{-3} become more closely spaced: the sensitivity to viscous damping becomes less appreciable as the surface Mach number is increased from 0.001 in Fig. 4(a) to 0.01 in Fig. 4(b). At low Mach numbers, the stabilizing role of viscosity appears to be more important in shorter motors. However, for a fixed set of physical properties, more elongated motors appear to be more susceptible to instabilities. This conclusion is supported by experimental observations reported by several investigators.[31,32] In Fig. 4(a), for example, the $\delta = 5\times10^{-4}$ curve predicts an unstable system for $L/R > 21$ at $m=1$ and $L/R > 42$ at $m=2$. Increasing viscous damping to $\delta = 10^{-3}$ delays instability until $L/R > 42$ at $m=1$ and $L/R > 84$ at $m=2$. This behavior is closely captured by Eq. (157) which predicts, for $M_b = 10^{-3}$, a critical $\xi_r \approx 2.646$. Despite being outside the asymptotic range of applicability for Eq. (157), one can solve for the critical length of motor l_r above which unstable conditions can prevail. This value is obtainable from

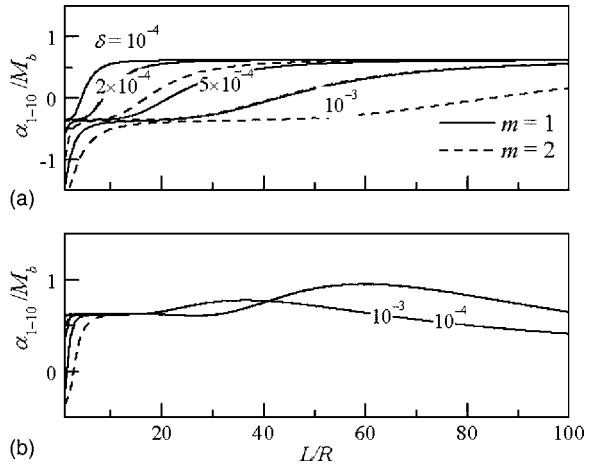

FIG. 4. Numerically integrated stability growth rate shown over a range of L/R and $m=1$, 2. Results are for two values of M_b corresponding to (a) 0.001 and (b) 0.01. In both cases, increasing δ or m increases system stability. Conversely, increasing the aspect ratio at fixed δ, m, and M_b moves the system in the direction of acoustic instability.

$$l_r = m\pi\delta\xi_r^{-1/2} M_b^{-3/2} \simeq \frac{m\pi\delta M_b^{-3/2}}{\sqrt{\frac{5}{6} + \frac{\sqrt{35}}{3}\sinh\left(\frac{1}{3}\sinh^{-1}\left\{4\left[\frac{325}{4} + 27\left(-\frac{15}{2} - 15\gamma_b\right)\right]/\left(35\sqrt{35}\right)\right\}\right)}}. \tag{164}$$

For $\delta = 5\times10^{-4}$, one finds $l_r = 30.5m$, thus providing an explanation for the doubling in critical chamber length when the mode number is increased to $m=2$. This result further supports the criticality of the fundamental oscillation mode given a finite chamber length.

As one would expect, higher oscillation modes play a stabilizing role insofar as they require more energy to excite. For rocket systems having $\delta < 10^{-3}$ and $M_b \approx 10^{-3}$, the fundamental mode ($m=1$) is seen to be the most critical. This result is reassuring because most studies concerned with predicting critical stability limits have routinely focused on the fundamental oscillation mode. Interestingly, this behavior can be corroborated through Eq. (155) given for α_{1-10}.

Figure 5 confirms that a more stable system is achieved when the viscous parameter ξ is increased. While the system is unstable in Fig. 5(a) at all practical Mach numbers, it is marginally stable in Fig. 5(b) and stable in Fig. 5(c). The influence of ξ on the magnitude of α_{1-10} is small in comparison with M_b. Nonetheless, the influence of ξ on the sign of α_{1-10} appears to be appreciable. These conclusions can also

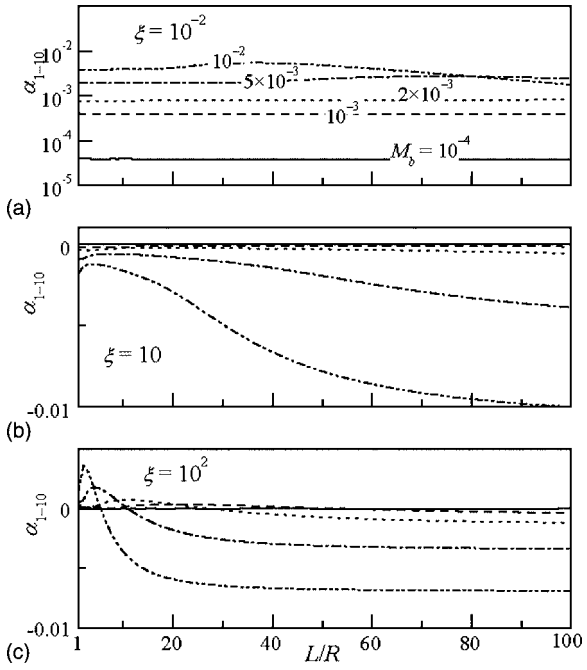

FIG. 5. Stability behavior for a range of L/R and M_b shown at (a) $\xi = 0.01$, (b) 10, and (c) 100 and $m=1$.

be reached by examining Figs. 5(a) and 5(b) where the composite solution is displayed at several Mach numbers and two practical aspect ratios.

Stability predictions based on the standard formulation are displayed in Fig. 6(c) for the same range of parameters. In all cases, the influence of ξ is increasingly more significant with progressive increases in M_b. The reason for this behavior may be connected to the impact that the ξM_b^2 term has on α_{1-10}; this impact is clearly captured in Eq. (155) for K_r.

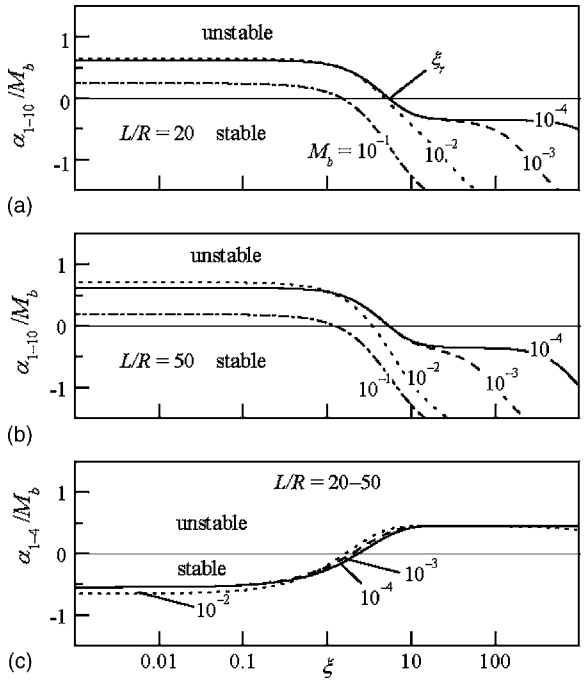

FIG. 6. Numerical stability curves at constant M_b shown over a useful range of ξ and select values of L/R. The system is more sensitive to the stabilizing role of ξ at the highest M_b. Here $A_b^{(r)}=1.75$, $\gamma=1.3$, and $m=1$.

The computational results of Fig. 6 support the existence of a critical value ξ_r which, when exceeded, will lead to a stable system—according to the rotational model [Figs. 6(a) and 6(b)]. However, an unstable system is predicted past a similar value ξ_i, according to the irrotational formulation [Fig. 6(c)]. The paradoxical behavior shown in Fig. 6(c) can be accurately reproduced from the analytical expression given by Eq. (148).

In Figs. 6(a) and 6(b), the critical values can be observed at $\xi_r \approx 5$ for $l=20$, and at $\xi_r \approx 3.5-5$ for $l=50$. According to the irrotational formulation, increasing viscous damping beyond a value of $\xi_i \approx 1.6-2.2$ leads to an unstable system for $l=20-50$.

It is interesting to note that, contrary to the standard prediction, the current stability curves shown in Figs. 6(a) and 6(b) usher an unstable system for $\xi < 1.6, \forall M_b, m, l$, and $A_b^{(r)}=1.75$. This explains, in part, the severe acoustic oscillations reported in many experimental tests in which the motors were assumed to be well within the stability bounds set forth by the standard model.

To isolate the effect of viscous damping, it is useful to examine the stability behavior versus $\delta=\sqrt{\nu/(a_0 R)}$. Unlike ξ, δ is not influenced by the chamber aspect ratio. Curves depicting the composite and standard formulations are compared in Fig. 7 over a range of δ and select values of l and M_b. As shown in Figs. 7(a) and 7(b), the chamber is more susceptible to instabilities when the aspect ratio or the Mach number is increased, or when δ is decreased. Most notably, the standard formulation predicts directly opposite trends, namely, an increased stability at larger Mach numbers or aspect ratios, and at smaller viscosity.

For $M_b=0.001$, the critical δ_r and δ_i that delineate the stability zones are obtained numerically and shown on the graphs. In connection with ξ_r or ξ_i, the corresponding δ_r and δ_i can be directly evaluated using $\delta=\xi^{1/2}M_b^{3/2}l/(m\pi)$ for a specific motor with given l, m, and M_b. Asymptotic approximations for these critical values are hence possible using, for example, Eq. (157). In fact, for the stated conditions, one calculates $\delta_r \approx (3\times10^{-4}, 8\times10^{-4})$ at $l=(20,50)$. These values compare favorably with their numerical counterparts shown in Figs. 7(a) and 7(b).

The stability outcome will markedly change when the admittance value is altered. The sensitivity to $A_b^{(r)}$ is critically important due to the strong dependence of the stability coefficients K_i and K_r on γ_b. This behavior is illustrated in Fig. 8 where both α_r and α_i are plotted at several representative values of $A_b^{(r)}$ (ranging from -2 to 5).

Each plot illustrates the solution at $l=20$ (full lines) and $l=50$ (broken lines) for both $M_b=0.001$ and 0.01. As one can extrapolate from Figs. 8(a) and 8(b), the sensitivity to increased motor length and M_b appears to be small when correlated versus ξ. The sensitivity to ξ is more appreciable, and becomes more significant at higher M_b. Increasing $A_b^{(r)}$ in the

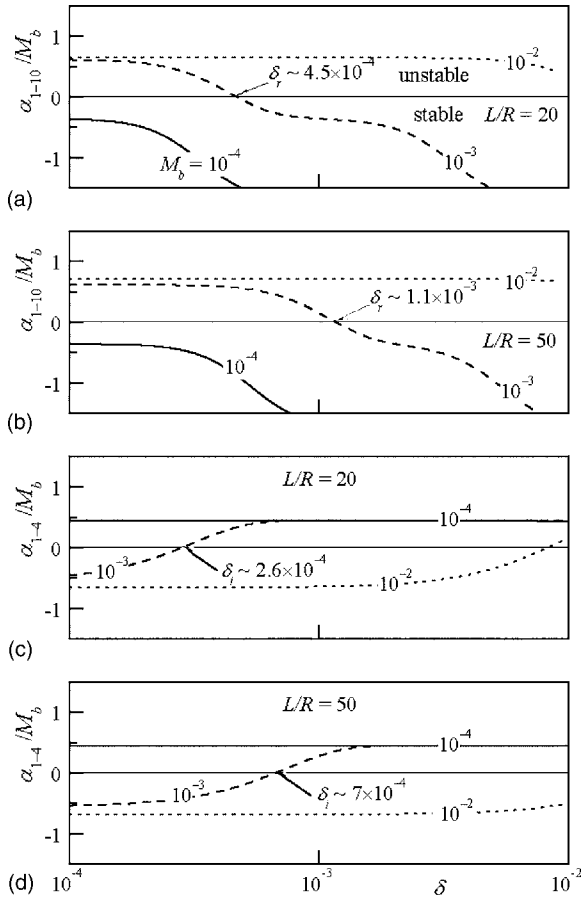

FIG. 7. Numerical stability curves at constant M_b shown over a useful range of δ and select values of L/R. The rotational formulation predicts a less stable system when δ is lowered or when L/R or M_b are increased. This explains, in part, the additional instabilities observed in elongated motors. The irrotational formulation predicts the opposite trends. Here $\gamma=1.3$ and $m=1$.

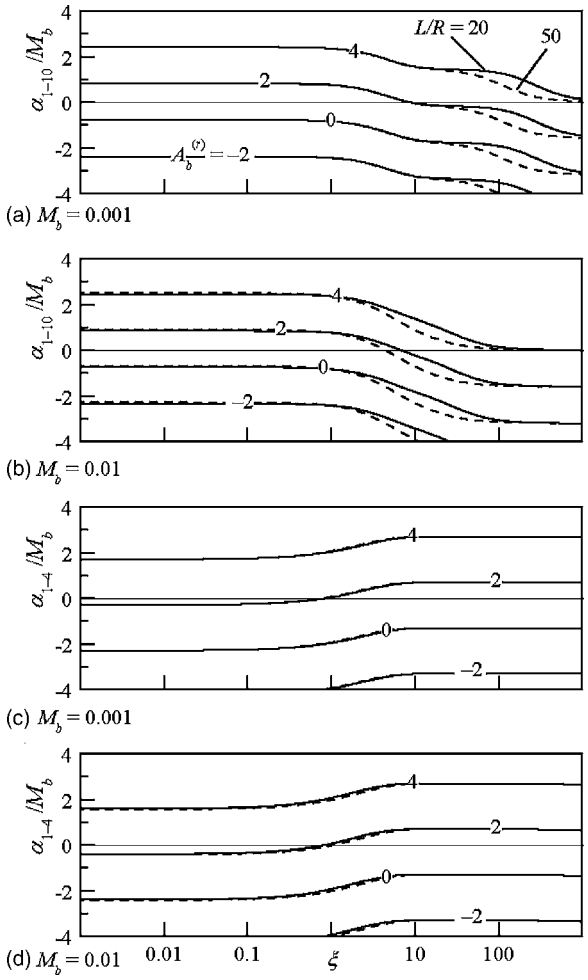

FIG. 8. Numerical stability curves shown at constant $A_b^{(r)}$ over a useful range of ξ and select values of M_b and L/R. Both rotational and irrotational formulations predict less stable systems with successive increases in $A_b^{(r)}$. However, they differ in their dependence on other parameters. Here $\gamma=1.3$ and $m=1$.

practical range from 1.0 to 2.5 causes an upward shift in the stability curves, thus requiring progressively more significant damping to maintain stable conditions.

In order to better depict the sensitivity to motor length, Mach number, and viscous levels, the stability curves are plotted versus δ (instead of ξ) in Fig. 9. An immediate realization is the reduced stability that can be associated with elongated motors ($l=50$) by comparison with shorter motors ($l=20$). Another result is the diminished stability at larger injection Mach numbers for which the sensitivity to motor aspect ratio is weakened. While the rotational formulation associates instability with increasing $M_b, L/R, A_b^{(r)}$ or with reducing δ, the irrotational model depicts contrasting trends. It may be interesting to note the visible deviations between rotational and irrotational stability curves over this particular range of $A_b^{(r)}$. Recalling that fundamental physical principles and experimental measurements tend to agree with the new model predictions concerning the destabilizing roles of $(M_b, L/R)$, and the damping (hence stabilizing) role of δ, current observations further amplify the need to adopt a fully rotational model.

E. Incorporating thermal effects

The growth rate factors presented here take into account most of the vortico-acoustic energy gains and losses present in the system. No account is taken, however, of the dilatational or thermal energy due to combustion, fluid-structure interactions, particle-mean flow coupling, and turbulence. In two recent studies by Chu, Yang, and Majdalani,[46] and Vyas, Majdalani, and Yang,[47] it is shown that thermal effects due to combustion can be incorporated into a nonreactive, isothermal model similar to the one used here. In summary, the key lies in increasing the blowing velocity at the wall (of a nonreactive model) such that it will match the velocity of the burning products directly above the flame zone. In these recent simulations,[46,47] it is shown that the flow outside the thin flame zone is virtually nonreactive and isothermal. Nonreactive models such as those developed by Majdalani and Flandro[14] become fairly adequate in the outer region occupied by the products. By setting the blowing speed in the nonreactive model equal to the thermally enhanced gas ejection speed at the edge of the flame zone, an excellent prediction capability can be achieved with the closed-form theoret-

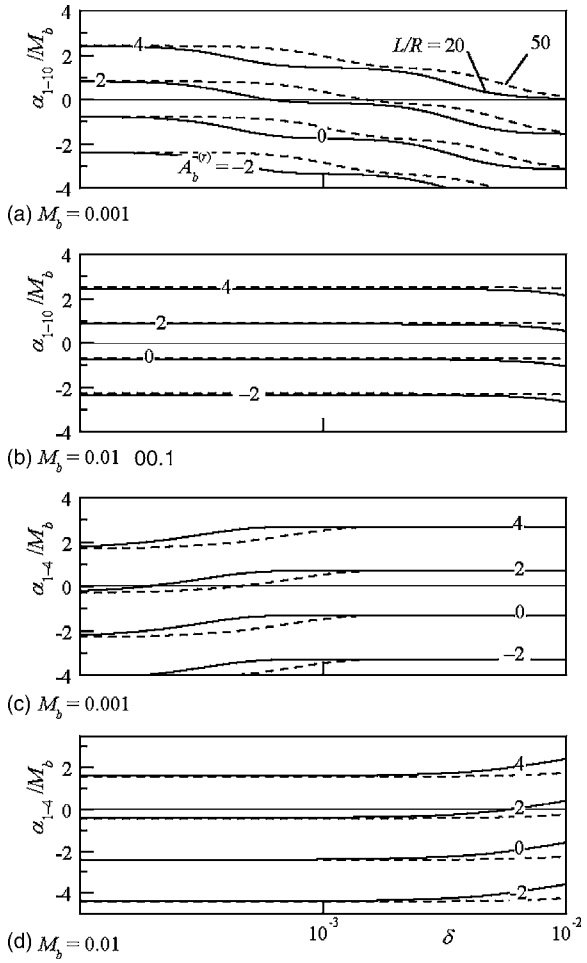

FIG. 9. Numerical stability curves shown at constant $A_b^{(r)}$ over a useful range of δ and select values of M_b and L/R. The rotational formulation associates acoustic instability with increasing $M_b, L/R, A_b^{(r)}$ or with reducing δ. Opposite trends are projected by the irrotational formulation. Here $\gamma = 1.3$ and $m = 1$.

ical solutions utilizing a higher effective Mach number. This adjustment helps to overcome one of the problems confronting analytical models such as those implemented at the foundation of the stability analysis developed here. The important effects of hydrodynamic instabilities, fluid structure, and particle-mean flow interactions are currently under investigation. It is hoped that additional correction factors will be further developed to account for other physical mechanisms excluded in the current study. Specifically, turbulence and particle damping appear to be critically important for the overall assessment of unsteady energy gains and losses in the combustion chamber.

V. CONCLUSION

By incorporating unsteady rotational terms in the energy balance, a higher-order formulation of the acoustic instability in rocket motors has been arrived at. The results constitute an extension to past formulations based on an irrotational representation of the acoustic field. The present formulation comprises six additional growth rate terms that have been discounted in irrotational stability models. These include corrections owing to the rotational flow, inviscid vortical, viscous, pseudoacoustical, pseudorotational, and unsteady nozzle effects.

Using four representative motors as case studies, predictions due to the unsteady rotational terms are shown to be non-negligible, thus justifying the dismissal of flow turning by means of the rotational flow correction and the inclusion of both inviscid vortical and small viscous corrections. The analytical expressions presented here are also shown to provide expeditious estimates of the volume integrals that arise in the stability calculations. Generally, the error in the analytical prediction has been shown to differ from the numerical solution by a few percent only.

The analytical expressions also lead to explicit relations between the main flow attributes and stability. This permits calculating critical motor lengths and Mach numbers that must not be exceeded, or critical damping levels that must be adhered to in order to mitigate acoustic instabilities. Physically, the proposed formulation agrees with basic principles and experimental findings by projecting a less stable environment with larger aspect ratios, with higher surface Mach numbers, and with higher surface admittance values. In the same vein, a more stable environment is promoted with higher oscillation mode numbers (which absorb more trigger energy) and with increasing amounts of viscous damping. These corrections, which have now been readily implemented into the SSP code,[11] provide suitable extensions to Culick's elegant framework. Not only do they bring into perspective contributions due to the unsteady vorticity and viscosity (α_6 and α_7), they also enable us to justify dismissing the flow turning, loss, thus achieving a formal reconciliation with other rigorous analyses.[34,35] As a windfall, they help to establish the secondary nature of the pseudopressure which, in the end, leads to either small corrections or factors that are offset by others.

Despite the progress made so far in the energy equation, more work lies ahead. Particularly, refinements are still needed to capture fluid-structure and particle-fluid interactions that can play an important role in stabilizing the system energy. A treatment of parietal vortex shedding (PVS) and intrinsic mean flow instabilities is also warranted in view of recent findings by Lupoglazoff and Vuillot,[31,32] and Griffond and Casalis.[48,49] There is overwhelming evidence that such instabilities can appear in the absence of inhibitors and intersegmental gaps, and lead to a new type of unstable waves exhibiting short wavelengths and propagating at much slower speeds than prescribed by acoustic motion. An excellent description of these waves and their contribution to the unsteady vorticity field are furnished by Griffond.[50]

ACKNOWLEDGMENTS

This work was sponsored by the Faculty Early Career Development (CAREER) Program of the National Science Foundation, under Grant No. CMS-0353518, Program Manager, Dr. Masayoshi Tomizuka. Grateful appreciation is expressed for additional University of Tennessee support from the Edward J. and Carolyn P. Boling Chair of Excellence in Advanced Propulsion, and the Jack D. Whitfield Professor-

ship of High Speed Flows. The authors thank Dr. Jonathan C. French, Software and Engineering Associates, Inc., for his valuable suggestions, and Dr. Fred S. Blomshield, Head of Combustion and Propulsion Research, Naval Air Warfare Center, for promoting cross-disciplinary research in this field.

[1]B.-T. Chu and L. S. G. Kovásznay, "Non-linear interactions in a viscous heat-conducting compressible gas," J. Fluid Mech. **3**, 494 (1957).
[2]F. E. C. Culick, "Acoustic oscillations in solid propellant rocket chambers," Astronaut. Acta **12**, 113 (1966).
[3]F. E. C. Culick, "Rotational axisymmetric mean flow and damping of acoustic waves in a solid propellant rocket," AIAA J. **4**, 1462 (1966).
[4]F. E. C. Culick, "Stability of longitudinal oscillations with pressure and velocity coupling in a solid propellant rocket," Combust. Sci. Technol. **2**, 179 (1970).
[5]F. E. C. Culick, "The stability of one-dimensional motions in a rocket motor," Combust. Sci. Technol. **7**, 165 (1973).
[6]F. E. C. Culick, "Stability of three-dimensional motions in a rocket motor," Combust. Sci. Technol. **10**, 109 (1974).
[7]R. L. Lovine, D. P. Dudley, and R. D. Waugh, Vols. I, II, and III Report No. AFRPL TR 76-32, 1976.
[8]G. R. Nickerson, F. E. C. Culick, and L. G. Dang, Report No. AFRPL TR-83-017, 1983.
[9]D. E. Coats and S. S. Dunn, "Improved motor stability predictions for 3D grains using the SPP code," in Proceedings of the 33rd AIAA/ASME/SAE/ASEE Joint Propulsion Conference (JPC), Seattle, WA, 1997.
[10]D. E. Coats and S. S. Dunn, Report No. SEA TR 95-02, 1995.
[11]J. C. French, G. A. Flandro, and J. Majdalani, "Improvements to the linear Standard Stability Prediction (SSP) program," in Proceedings of the 40th AIAA/ASME/SAE/ASEE Joint Propulsion Conference, Fort Lauderdale, FL, 2004.
[12]F. E. C. Culick, "Rotational axisymmetric mean flow and damping of acoustic waves in a solid propellant rocket," J. Propul. Power **5**, 657 (1989).
[13]G. A. Flandro, AIAA Report No. 95-2530, 1995.
[14]J. Majdalani and G. A. Flandro, "The oscillatory pipe flow with arbitrary wall injection," Proc. R. Soc. London, Ser. A **458**, 1621 (2002).
[15]G. A. Flandro, "Effects of vorticity on rocket combustion stability," J. Propul. Power **11**, 607 (1995).
[16]G. A. Flandro, W. Cai, and V. Yang, in *Solid Propellant Chemistry, Combustion, and Motor Interior Ballistics*, edited by V. Yang, T. B. Brill, and W.-Z. Ren (AIAA Progress in Astronautics and Aeronautics, Washington, DC, 2000), Vol. 185, pp. 837–858.
[17]J. Majdalani, G. A. Flandro, and T. S. Roh, "Convergence of two flowfield models predicting a destabilizing agent in rocket combustion," J. Propul. Power **16**, 492 (2000).
[18]J. Majdalani and W. K. Van Moorhem, "Improved time-dependent flowfield solution for solid rocket motors," AIAA J. **36**, 241 (1998).
[19]J. Majdalani, "The boundary layer structure in cylindrical rocket motors," AIAA J. **37**, 505 (1999).
[20]J. Majdalani, "Vorticity dynamics in isobarically closed porous channels. Part I: Standard perturbations," J. Propul. Power **17**, 355 (2001).
[21]J. Majdalani and T. S. Roh, "Vorticity dynamics in isobarically closed porous channels. Part II: Space-reductive perturbations," J. Propul. Power **17**, 363 (2001).
[22]J. Majdalani and T. S. Roh, "The oscillatory channel flow with large wall injection," Proc. R. Soc. London, Ser. A **456**, 1625 (2000).
[23]F. Vuillot and G. Avalon, "Acoustic boundary layer in large solid propellant rocket motors using Navier–Stokes equations," J. Propul. Power **7**, 231 (1991).
[24]T. S. Roh, I. S. Tseng, and V. Yang, "Effects of acoustic oscillations on flame dynamics of homogeneous propellants in rocket motors," J. Propul. Power **11**, 640 (1995).
[25]V. Yang and T. S. Roh, in Proceedings of the 31st AIAA/ASME/SAE/ASEE Joint Propulsion Conference, San Diego, CA, 1995.
[26]F. Vuillot, "Numerical computation of acoustic boundary layers in large solid propellant space booster," in Proceedings of the 29th Aerospace Sciences Meeting, Reno, NV, 1991.
[27]J. D. Baum, J. N. Levine, and R. L. Lovine, "Pulsed instabilities in rocket motors: A comparison between predictions and experiments," J. Propul. Power **4**, 308 (1988).
[28]J. D. Baum, in Proceedings of the 25th AIAA/ASME/SAE/ASEE Joint Propulsion Conference, Monterey, CA, 1989.
[29]C. W. Shaeffer and R. S. Brown, AFOSR Contract No. F04620-90-C-0032, 1990.
[30]C. W. Shaeffer and R. S. Brown, Chemical Systems Div. No. 2060 FR, 1992.
[31]N. Lupoglazoff and F. Vuillot, "Parietal vortex shedding as a cause of instability for long solid propellant motors. Numerical simulations and comparisons with firing tests," in Proceedings of the 34th Aerospace Sciences Meeting, Reno, NV, 1996.
[32]N. Lupoglazoff and F. Vuillot, "Numerical simulations of parietal vortex-shedding phenomenon in a cold-flow set-up," in Proceedings of the 34th AIAA/ASME/SAE/ASEE Joint Propulsion Conference, Cleveland, OH, 1998.
[33]G. A. Flandro and J. Majdalani, "Aeroacoustic instability in rockets," AIAA J. **41**, 485 (2003).
[34]W. K. Van Moorhem, "Flow turning in solid-propellant rocket combustion stability analyses," AIAA J. **20**, 1420 (1982).
[35]W. K. Van Moorhem, "An investigation of the origin of the flow turning effect in combustion instability," in 17th Joint Army Navy NASA Air Force (JANNAF) Combustion Conference, Langley, VA, 1980.
[36]J. Majdalani and W. K. Van Moorhem, "Laminar cold-flow model for the internal gas dynamics of a slab rocket motor," Aerosp. Sci. Technol. **5**, 193 (2001).
[37]N. Lupoglazoff and F. Vuillot, "Numerical simulation of vortex shedding phenomenon in two-dimensional test case solid rocket motors," in Proceedings of the 30th Aerospace Sciences Meeting, Reno, NV, 1992.
[38]F. Vuillot, "Vortex-shedding phenomena in solid rocket motors," J. Propul. Power **11**, 626 (1995).
[39]J. Dupays, M. Prévost, P. Tarrin, and F. Vuillot, "Effects of particulate phase on vortex shedding driven oscillations in solid rocket motors," in Proceedings of the 32nd AIAA/ASME/SAE/ASEE Joint Propulsion Conference, Orlando, FL, 1996.
[40]J. Dupays, "Contribution à l'Étude du Rôle de la Phase Condensée dans la Stabilité d'un MPS pour Lanceur Spatial," Ph.D. dissertation, ONERA, 1996.
[41]W.-W. Chu, V. Yang, and J. Majdalani, "Premixed flame response to acoustic waves in a porous-walled chamber with surface mass injection," Combust. Flame **133**, 359 (2003).
[42]A. B. Vyas, J. Majdalani, and V. Yang, "Estimation of the laminar premixed flame temperature and velocity in injection-driven combustion chambers," Combust. Flame **133**, 371 (2002).
[43]G. Kirchoff, *Vorlesungen Über Mathematische Physik: Mechanik*, 2nd ed. (Teubner, Leibzig, 1877).
[44]G. Avalon and P. Comas, "Simulative study of the unsteady flow inside a solid propellant rocket motor," in Proceedings of the 27th AIAA/ASME/SAE/ASEE Joint Propulsion Conference, Sacramento, CA, 1991.
[45]R. S. Brown, R. Dunlap, S. W. Young, and R. C. Waugh, "Vortex shedding as a source of acoustic energy in segmented solid rockets," J. Spacecr. Rockets **18**, 312 (1981).
[46]W.-W. Chu, V. Yang, and J. Majdalani, "Premixed flame response to acoustic waves in a porous-walled chamber with surface mass injection," Combust. Flame **133**, 359 (2003).
[47]A. B. Vyas, J. Majdalani, and V. Yang, "Estimation of the laminar premixed flame temperature and velocity in injection-driven combustion chambers," Combust. Flame **133**, 371 (2003).
[48]J. Griffond and G. Casalis, "On the nonparallel stability of the injection induced two-dimensional Taylor flow," Phys. Fluids **13**, 1635 (2001).
[49]J. Griffond and G. Casalis, "On the dependence on the formulation of some nonparallel stability approaches applied to the Taylor flow," Phys. Fluids **12**, 466 (2000).
[50]J. Griffond, "Receptivity and aeroacoustic resonance in channels with blowing walls," Phys. Fluids **14**, 3946 (2002).